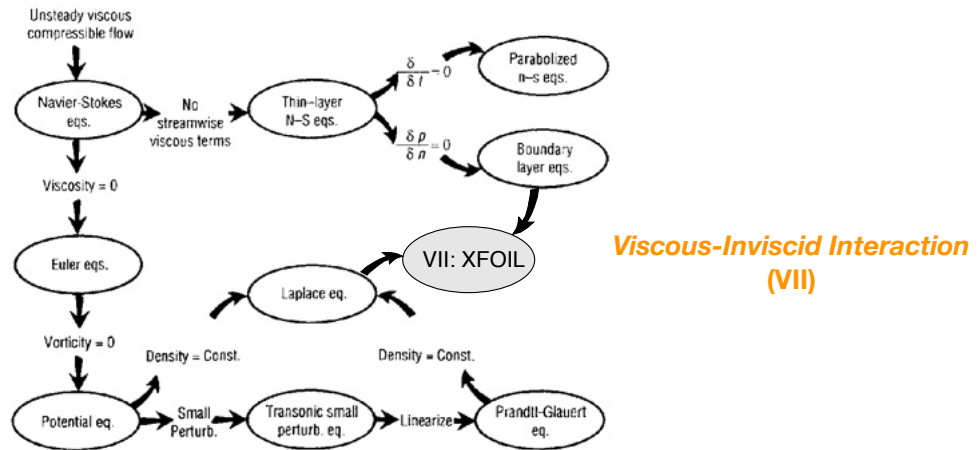
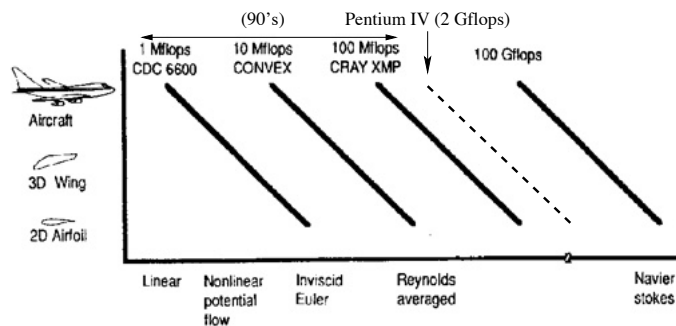


Airfoil analysis and design

Hierarchy of flow models with simplifying assumptions



Flow model complexity versus cost of analysis



Airfoil analysis versus design

The aerospace engineer could face an aerodynamical problem in two forms:

1. **Analysis:** the Direct Problem

What are the aerodynamic characteristics of a given airfoil shape?

2. **Design:** the Inverse Problem

What is the airfoil shape that leads to given aerodynamic characteristics?

We will look at the tools for both tasks.

The basic presumption of most wing analysis and design is that the flow local to each section of the wing is approximately 2D. This enables us to focus on 2D profile design more-or-less independently of finite-wing effects.

Drela (1990):

... resolving wing profile design conflicts is far more effective when done at the 2D level.

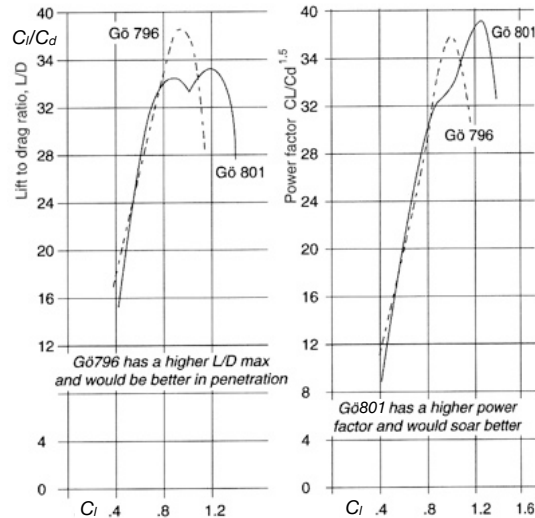
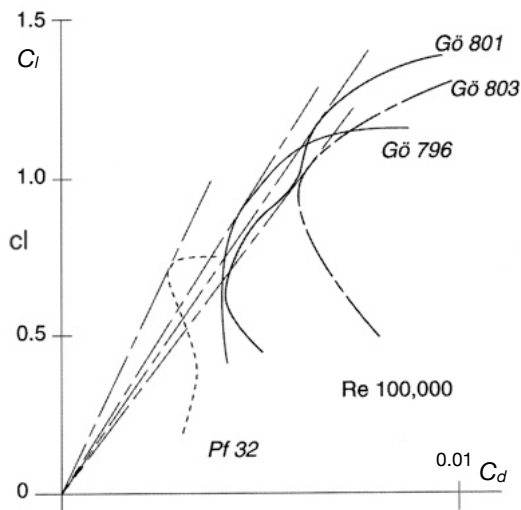
Liebeck (1990):

Stated in simple form, the minimum requirements for an airfoil are that it is non-re-entrant, has a rounded leading edge, and has a pointed trailing edge.

How do we assess airfoil performance?

A broad-brush approach looks at the airfoil performance as a whole, based on the drag polar and measures derived from this — e.g. $(C_l/C_d)_{\max}$, $(C_l^{1/2}/C_d)_{\max}$, $(C_l^{3/2}/C_d)_{\max}$.

[Used to compare/select airfoils.](#)



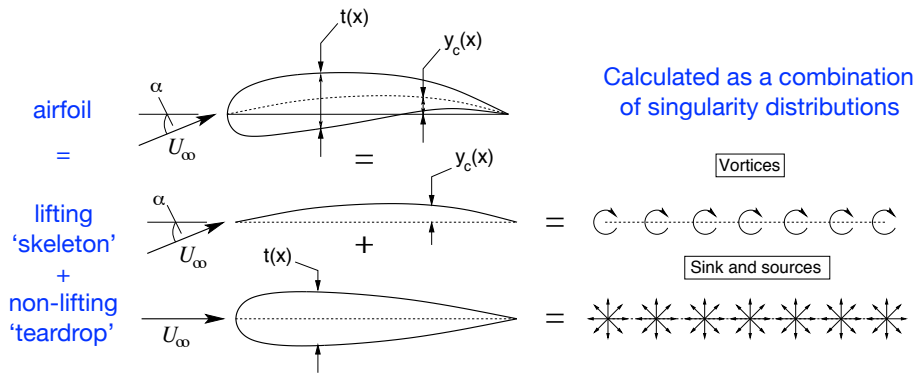
Finer-scale measures look more carefully to the underlying causes of specific performance aspects, e.g.:

1. Low drag (C_d) over design lift coefficient range (C_l);
2. Turbulent transition and drag (for laminar flow airfoils);
3. Mach number sensitivity (transonic drag rise);
4. Reynolds number sensitivity;
5. Simple flap/aileron effects;
6. Surface waviness tolerance (to transition).

[Used in airfoil design.](#)

Inviscid methods for airfoil analysis and design

Thin airfoil theory



Calculated as a combination of singularity distributions

For simplicity it is here assumed that the vorticity γ lies along the chord line **but** it has the correct strength to match the flow to the mean camber line.

Vortex-sheet analysis for lifting skeleton

Linearize, α small

$$u = U_\infty + u'$$

$$v = U_\infty \alpha + v'$$

No flow normal to mean camber line:

$$U_\infty \left(\alpha - \frac{dy_c}{dx} \right) + v' = 0$$

Assume potential flow

$$u' = \frac{\partial \phi}{\partial x}$$

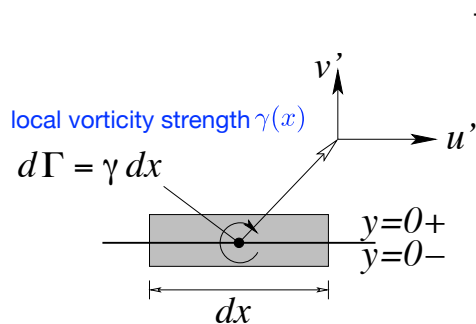
$$v' = \frac{\partial \phi}{\partial y}$$

$$\nabla^2 \phi = 0$$

— superposition is valid

Lifting solution — direct method — 1

Calculate $C_p(x)$ for a cambered airfoil skeleton with zero thickness, $y=y_c(x)$. (Say chord $c=1$.)



The aerodynamic characteristics are

$$u'(x, 0^\pm) = \pm \frac{\gamma}{2}$$

$$v'(x, 0) = -\frac{1}{2\pi} \int_0^c \gamma(\xi) \frac{d\xi}{x - \xi}$$

$$C_p = \mp \frac{\gamma}{U_\infty}$$

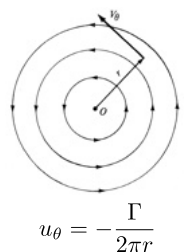
$$C_l = \frac{2}{U_\infty c} \int_0^c \gamma(\xi) d\xi$$

via Biot-Savart

$$C_p = 1 - \left(\frac{U}{U_\infty} \right)^2$$

$$= 1 - \left(\frac{U_\infty + u'}{U_\infty} \right)^2$$

recall for a discrete vortex



The strength per unit length $\gamma(x)$ of the distribution of vorticity along the chord line is now obtained by solving the flow tangency condition

$$U_\infty \left(\alpha - \frac{dy_c}{dx} \right) + v'(x) = 0; \quad \text{with } \gamma(1) = 0$$

Kutta condition, i.e. $u'=0$ at TE

The final equation is

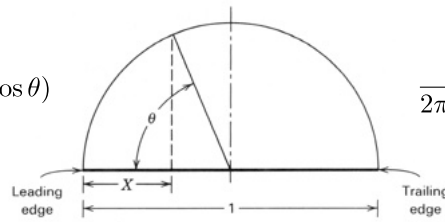
$$U_\infty \left(\alpha - \frac{dy_c}{dx} \right) - \frac{1}{2\pi} \int_0^1 \gamma(\xi) \frac{d\xi}{x - \xi} = 0; \quad \text{with } \gamma(1) = 0$$

this has to be solved for $\gamma(x)$ given the shape y_c .

Lifting solution – direct method – 2

Solution: (by Betz)

Apply the mapping $x = \frac{1}{2}(1 - \cos \theta)$



$$\frac{1}{2\pi U_\infty} \int_0^\pi \frac{\gamma(\theta) \sin \theta d\theta}{\cos \theta - \cos \theta(x)} = \alpha - \frac{dy_c(x)}{dx}$$

The vorticity distribution at $\alpha \neq 0$ is singular like $1/x$, and is assumed to have a Fourier-type expansion

$$\gamma(x) = 2U_\infty \left(A_0 \frac{1 + \cos \theta}{\sin \theta} + \sum_{n=1}^{\infty} A_n \sin n\theta \right)$$

Use the relationships

$$\frac{1}{2} [\cos(n-1)\theta - \cos(n+1)\theta] = \sin n\theta \sin \theta \quad \text{and} \quad \int_0^\pi \frac{\cos n\theta d\theta}{\cos \theta - \cos \theta(x)} = \pi \frac{\sin n\theta(x)}{\sin \theta(x)}$$

to obtain

$$A_0 - \sum_{n=1}^{\infty} A_n \cos n\theta = \alpha - \frac{dy_c}{dx}(x)$$

Multiply both sides by $\cos m\theta$, integrate from 0 to π , obtain A_n as

$$A_0 = \alpha - \frac{1}{\pi} \int_0^\pi \frac{dy_c}{dx}(\theta) d\theta \quad A_n = \frac{2}{\pi} \int_0^\pi \frac{dy_c}{dx}(\theta) \cos n\theta d\theta$$

So for any camber line we can obtain the full set of coefficients.

Lifting solution – direct method – 3

Using the Kutta-Joukowski relationship $L = \rho U_\infty \Gamma$

$$L = \int_0^1 \rho U_\infty \gamma(x) dx \quad \text{and} \quad M_{LE} = \int_0^1 \rho U_\infty \gamma(x) x dx$$

Lift

$$C_l = 2\pi A_0 + \pi A_1 \quad \text{and}$$

$$\frac{\partial C_l}{\partial \alpha} = 2\pi$$

Moment

$$C_{m_{LE}} = -\frac{\pi}{2} \left(A_0 + A_1 - \frac{A_2}{2} \right)$$

now using statics (and a small, $C_d=0$) we had $C_{m_x} = C_{m_a} - C_l \left(\frac{x}{c} - \frac{a}{c} \right)$ so

$$C_{m_{c/4}} = \frac{\pi}{4} (A_2 - A_1) \quad (\text{independent of } \alpha).$$

(Zero for a symmetrical section. i.e. $A_1=A_2$.)

These are two fundamental results of thin-airfoil theory.

Lifting solution – inverse method

Calculate the camber line $y=y_c(x)$ that produces a given pressure distribution $C_p(x)$.

From

$$v'(x, 0) = -\frac{1}{2\pi} \int_0^c \gamma(\xi) \frac{d\xi}{x - \xi}$$

$$C_p = \mp \frac{\gamma}{U_\infty}$$

we have

$$v'(x) = -\frac{1}{2\pi} \int_0^c U_\infty C_p(\xi) \frac{d\xi}{x - \xi}$$

and the shape of the camber line is obtained by integration of the flow tangency equation

$$U_\infty \left(\alpha - \frac{dy_c}{dx} \right) + v'(x) = 0$$

as

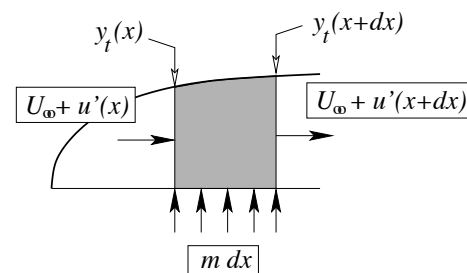
$$y_c(x) = \alpha x + \int_0^x \frac{v'(\xi)}{U_\infty} d\xi$$

Non-lifting solution – direct method

Calculate $C_p(x)$ for a thin symmetric airfoil with a thickness distribution $y=\pm y_t(x)/2$.

(i) Airfoil surface is a streamline – by definition no flow crosses a streamline.

(ii) Flow internal to the streamline is created by source-sink distribution, local strength m .



Conservation of mass: $m = 2U_\infty \frac{dy_t}{dx}$

The aerodynamic characteristics are:

$$u'(x, 0) = \frac{U_\infty}{\pi} \int_0^c m(\xi) \frac{d\xi}{x - \xi}$$

$$v'(x, 0\pm) = \pm \frac{m}{2}$$

$$C_p = -\frac{2u'}{U_\infty}$$

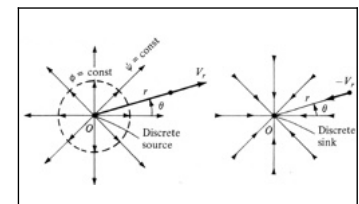
For instance, for an elliptic airfoil:

$$y_t = \pm t \sqrt{x - (c - x)}$$

$$\frac{dy_t}{dx} = \pm \frac{t}{2} \frac{c - 2x}{\sqrt{x(c - x)}}$$

$$C_p = -2t$$

Recall for a discrete source or sink:



$$u_r = \pm \frac{\Lambda}{2\pi r}$$

Non-lifting solution – inverse method

Calculate thickness distribution $y_t(x)$ that gives $C_p(x)$.

Recall: $C_p = -\frac{2u'}{U_\infty}$

$$u'(x, 0) = \frac{U_\infty}{\pi} \int_0^c \frac{dy_t}{dx}(\xi) \frac{d\xi}{x - \xi}$$

This amounts to solving the equation:

$$C_p(x) = -\frac{2}{\pi} \int_0^c \frac{dy_t}{dx}(\xi) \frac{d\xi}{x - \xi}$$

which can be done using Fourier series expansions for both y_t and C_p or, using a result by Betz, by direct integration of

$$\frac{dy_t}{dx} = \frac{1}{2\pi} \int_0^c C_p(x) \sqrt{\frac{\xi(c - \xi)}{x(c - x)}} \frac{d\xi}{x - \xi}$$

Riegels' correction

The velocity distribution given by the theory,

$$\frac{u}{U_\infty} = 1 + \frac{1}{\pi} \int_0^c \frac{dy_t}{dx}(\xi) \frac{d\xi}{x - \xi}$$

is very inaccurate near rounded LEs, where $dy_t/dx \rightarrow \infty$, as then does u .

Riegels proposed a correction for the velocity which works for thicker airfoils

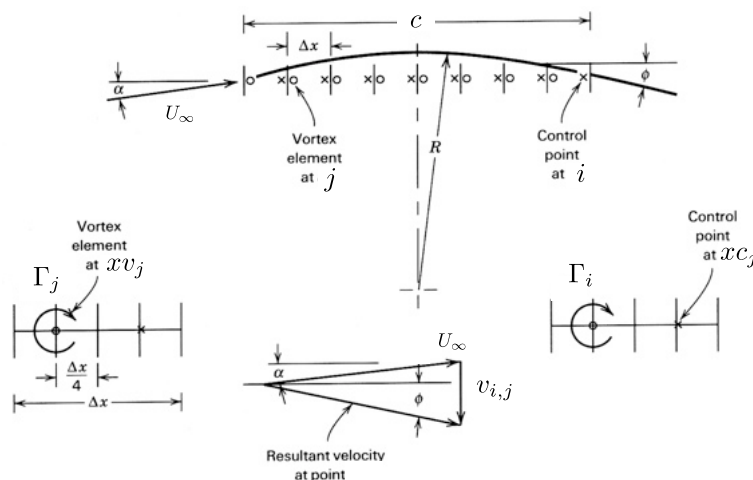
$$\frac{u}{U_\infty} = \left\{ 1 + \left[\frac{dy_t}{dx} \right]^2 \right\}^{-1/2} \left(1 + \frac{1}{\pi} \int_0^c \frac{dy_t}{dx}(\xi) \frac{d\xi}{x - \xi} \right)$$

The first term (the correction) $\rightarrow 0$ as $dy_t/dx \rightarrow \infty$.

Discrete direct methods for thin airfoils – 1

Now consider the discrete equivalent to finding the direct thin-airfoil continuum solution: given a camber line of arbitrary shape, determine the vorticity distribution, lift, moment...

1. Break the **chord** line up into N line segments. We place a discrete vortex of strength Γ at the $1/4$ -chord point of each segment and a control point (where we determine velocity) at the $3/4$ -chord point.



2. The *downward* velocity induced at the i th control point located at $x c_i$ by the j th discrete vortex of strength Γ_j located at $x v_j$ is

$$v'_{i,j} = \frac{\Gamma_j}{2\pi(x c_i - x v_j)} \quad \left(\text{recall } u_\theta = -\frac{\Gamma}{2\pi r} \text{ for potential flow} \right)$$

NB: vortices and control points are located on the chord line, just as in the continuous case.

Discrete direct methods for thin airfoils – 2

3. The vector sum of the total induced vertical velocity and the oncoming flow has to be tangent to the **camber line** at each control point location i , as stated by

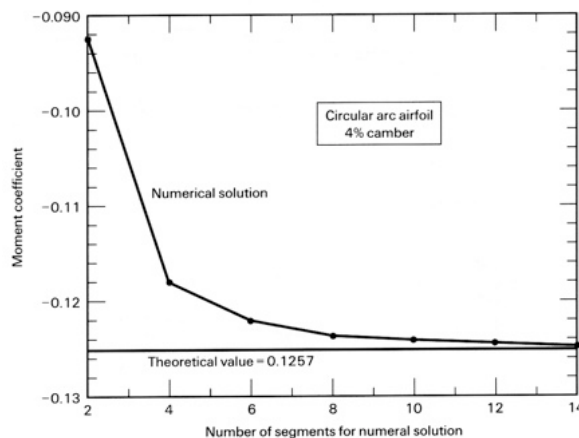
Each control point i generates one equation.
$$\sum_{j=1}^N \frac{\Gamma_j}{2\pi[xc_i - xv_j]} = U_\infty \left[\alpha - \frac{dy_c}{dx} \Big|_i \right]$$
 This is the discrete version of the flow tangency condition.

4. This gives N simultaneous linear equations that we can solve for the unknown Γ_j s.

5. From these we can obtain lift and moment coefficients, etc:

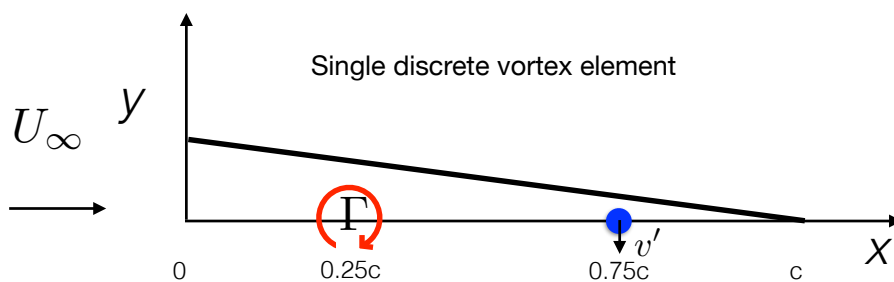
$$C_l = \frac{2}{U_\infty c} \sum_{i=1}^N \Gamma_i, \quad C_{m_{LE}} = -\frac{2}{U_\infty c^2} \sum_{i=1}^N xv_i \Gamma_i, \quad C_{m_{c/4}} = C_{m_{LE}} + C_l/4$$

6. These converge to the continuous solution as $N \rightarrow \infty$.



In fact for the particular locations of vortex and control points used, we get the exact C_l , regardless of N (including $N=1$, i.e. just one vortex), provided the camber line is continuous at $0.75c$.

Easy example: flat plate



Velocity induced at collocation point

$$v'_{i,j} = \frac{\Gamma_j}{2\pi(xc_i - xv_j)} \longrightarrow v' = \Gamma / 2\pi(0.5c)$$

Flow tangent to flat plate

$$v' = U_\infty \alpha \longrightarrow \Gamma = \pi U_\infty \alpha c$$

Lift coefficient

$$C_l = \frac{2}{U_\infty c} \Gamma = 2\pi\alpha$$

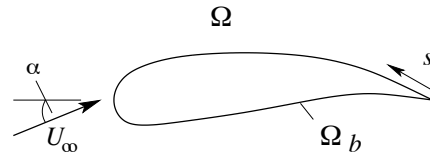
This result matches the theoretical result, but this only occurs with this trivial example. A higher number of vortices and control points is usually required for different cambers.

2D Panel Method: direct method – 1

Now we consider the problem of directly computing the potential flow without thin-airfoil assumptions.

1. We consider potential flows governed by the Laplace equation with 'no flow through' boundary conditions at surfaces.

$$\nabla^2 \phi = 0 \quad \text{in } \Omega; \quad \mathbf{V} \cdot \mathbf{n} = \frac{\partial \phi}{\partial n} = 0 \quad \text{on } \Omega_b$$



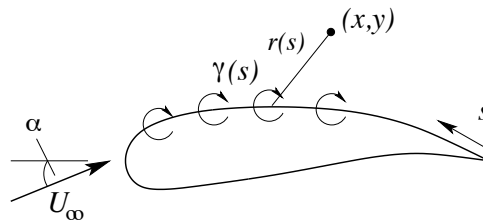
2. Also we have to satisfy the Kutta condition, so that the flow leaves tangentially at the TE, or, if the TE angle is finite, at the average tangency.

3. The solution is obtained by linearly superimposing basic solutions, for example vortex flow, which has (in r - θ polar coordinates):

$$\phi = -\frac{\Gamma}{2\pi}\theta; \quad \psi = \frac{\Gamma}{2\pi}\ln r; \quad v_\theta = -\frac{\Gamma}{2\pi r}; \quad v_r = 0.$$

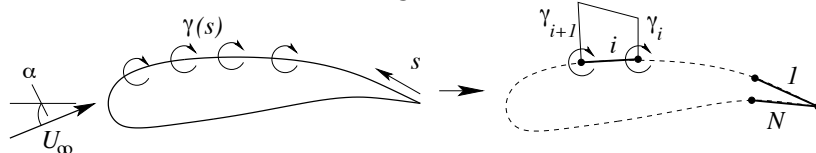
4. Assuming a distribution of vortex sheet strength $\gamma(s)$ along the perimeter length s of the airfoil, the velocity potential at any location corresponding to an incidence α is

$$\phi(x, y) = U_\infty(x \cos \alpha + y \sin \alpha) - \frac{1}{2\pi} \oint \gamma(s) \arctan \left(\frac{y - y(s)}{x - x(s)} \right) ds$$



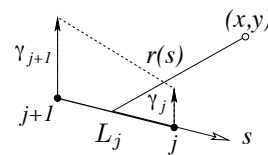
2D Panel Method: direct method – 2

5. To calculate the integral approximately, divide the airfoil surface into N discrete panels, with piecewise-linear distribution of vortex sheet strength



The vortex sheet strength on a single panel is

$$\gamma(s_j) = \gamma_j + (\gamma_{j+1} - \gamma_j) \frac{s_j}{L_j}$$



6. We add up all the contributions to velocity potential and then differentiate to obtain velocities.
7. By imposing zero flow normal to the airfoil at a set of N control points we obtain N equations

$$\sum_{j=1}^N K_{ij} \gamma_j = U_\infty \cdot \mathbf{n}_i \quad i = 1, 2, \dots, N$$

Here we have N equations and $N+1$ unknowns (values of γ_j). The influence coefficients K_{ij} are obtained from the integrals above.

8. An additional equation that closes the system is obtained from the Kutta condition by adding an equation for the TE strengths

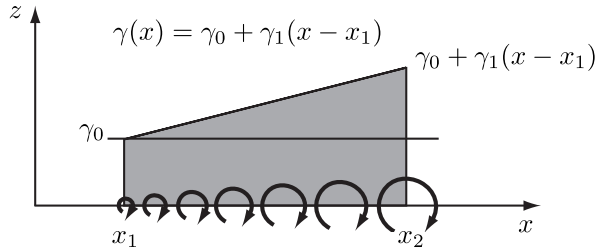
$$\gamma_1 + \gamma_{N+1} = 0$$

In continuum mechanics, panel methods are called 'boundary element methods' – a special kind of finite element method.

2D Panel Method: direct method – 3

Details for linear-strength vortex panel (Katz & Plotkin chapters 10, 11, Kuethe & Chow chapter 5).

1. Start in panel coordinate system, vortex sheet strength $\gamma(x)$.



$$\phi(x, z) = -\frac{\gamma_0}{2\pi} \int_{x_1}^{x_2} \tan^{-1} \left(\frac{z}{x - x_0} \right) dx_0 - \frac{\gamma_1}{2\pi} \int_{x_1}^{x_2} x_0 \tan^{-1} \left(\frac{z}{x - x_0} \right) dx_0$$

2. Integrate to obtain:

$$\phi(x, z) = -\frac{\gamma_0}{2\pi} \left[(x - x_1) \tan^{-1} \left(\frac{z}{x - x_1} \right) - (x - x_2) \tan^{-1} \left(\frac{z}{x - x_2} \right) + \frac{z}{2} \ln \frac{(x - x_1)^2 + z^2}{(x - x_2)^2 + z^2} \right] - \frac{\gamma_1}{2\pi} \left[\frac{xz}{2} \ln \frac{(x - x_1)^2 + z^2}{(x - x_2)^2 + z^2} - \frac{z}{2} (x_1 - x_2) + \frac{x^2 - x_1^2 - z^2}{2} \tan^{-1} \left(\frac{z}{x - x_1} \right) - \frac{x^2 - x_2^2 - z^2}{2} \tan^{-1} \left(\frac{z}{x - x_2} \right) \right]$$

3. Let

$$r_1 = \sqrt{(x - x_1)^2 + z^2}, \quad \theta_1 = \tan^{-1} \frac{z}{x - x_1}$$

$$r_2 = \sqrt{(x - x_2)^2 + z^2}, \quad \theta_2 = \tan^{-1} \frac{z}{x - x_2}$$

$$\gamma_a = \gamma_0, \quad \gamma_b = \gamma_0 + \gamma_1(x_2 - x_1)$$

4. Differentiate the velocity potential to obtain panel-induced velocity components (u_p, w_p) at collocation point (x_c, z_c) :

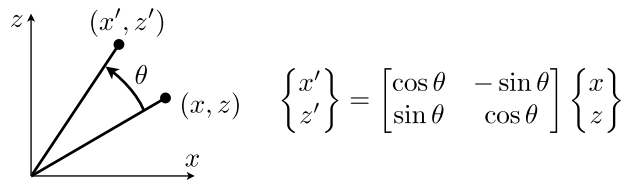
$$u_p = \frac{z_c}{2\pi} \left(\frac{\gamma_b - \gamma_a}{x_2 - x_1} \right) \ln \frac{r_2}{r_1} + \frac{\gamma_a(x_2 - x_1) + (\gamma_b - \gamma_a)(x_c - x_1)}{2\pi(x_2 - x_1)} (\theta_2 - \theta_1),$$

$$w_p = \frac{\gamma_a(x_2 - x_1) + (\gamma_b - \gamma_a)(x_c - x_1)}{2\pi(x_2 - x_1)} \ln \frac{r_2}{r_1} + \frac{z_c}{2\pi} \left(\frac{\gamma_b - \gamma_a}{x_2 - x_1} \right) \left[\frac{x_2 - x_1}{z_c} + (\theta_1 - \theta_2) \right]$$

2D Panel Method: direct method – 4

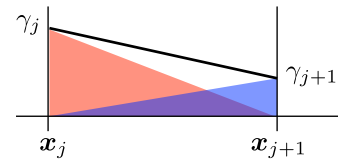
5. We need N panels to cover the airfoil. In general, for the j th panel, we can use the substitutions $\gamma_a \rightarrow \gamma_j, \gamma_b \rightarrow \gamma_{j+1}, x_1 \rightarrow x_j, x_2 \rightarrow x_{j+1}, \theta_1 \rightarrow \theta_j, \theta_2 \rightarrow \theta_{j+1}$.

6. The velocity components (u_p, w_p) were derived in the panel coordinate system. We need to transform/rotate both the given end points $(x_j, z_j), (x_{j+1}, z_{j+1})$ for any panel as well as the collocation point of interest (x_i, z_i) from global to local coordinates, then transform the velocity components at any collocation point location back to global coordinates. Use direction cosine matrices:



7. We can break the collocation point velocity $(u, w)(x_i, z_i)$ induced by the distribution of vorticity on panel j into two parts, each with a triangular shape function:

- (i) $(u_a, w_a)(x_i, z_i) \leftarrow$ part related just to γ_j
- (ii) $(u_b, w_b)(x_i, z_i) \leftarrow$ part related just to γ_{j+1}



8. Then implement all of the above via a subroutine that takes the j th panel end-coordinates (x_j, x_{j+1}) and (x_{j+1}, z_{j+1}) and the location of the i th control point (x_i, z_i) , and returns the global-coordinate velocity components $(u_a, w_a)(x_i, z_i)$ and $(u_b, w_b)(x_i, z_i)$ given unit strengths γ_j and γ_{j+1} for the panel-end vorticity distribution.

```

procedure vort2d1 (real    x1, z1, x2, z2, // -- panel-end coordinates
                  (real    xc, zc, // -- collocation-point coordinates
                  (var real ua, wa, ub, wb) // -- output velocity components

```

2D Panel Method: direct method – 5

9. At the first control point there will be contributions from each of the panels:

$$(u, w)_1 = (u_a, w_a)_{1,1} \gamma_1 + [(u_b, w_b)_{1,1} + (u_a, w_a)_{1,2}] \gamma_2 + [(u_b, w_b)_{1,2} + (u_a, w_a)_{1,3}] \gamma_3 + \dots + [(u_b, w_b)_{1,N-1} + (u_a, w_a)_{1,N}] \gamma_N + (u_b, w_b)_{1,N} \gamma_{N+1}$$

And for the i th control/collocation point:

$$(u, w)_i = (u_a, w_a)_{i,1} \gamma_1 + [(u_b, w_b)_{i,1} + (u_a, w_a)_{i,2}] \gamma_2 + [(u_b, w_b)_{i,2} + (u_a, w_a)_{i,3}] \gamma_3 + \dots + [(u_b, w_b)_{i,N-1} + (u_a, w_a)_{i,N}] \gamma_N + (u_b, w_b)_{i,N} \gamma_{N+1}$$

$$= (u_a, w_a)_{i,1} \gamma_1 + \sum_{j=2}^N [(u_b, w_b)_{i,j-1} + (u_a, w_a)_{i,j}] \gamma_j + (u_b, w_b)_{i,N} \gamma_{N+1}$$

$$\equiv \sum_{j=1}^{N+1} (u, w)_{i,j} \gamma_j \quad \text{This is one of a system of equations (a row in a matrix).}$$

10. We want the not the velocity at the control points but the panel-normal component of the velocity (which we will set to zero): $K_{i,j} = (u, w)_{i,j} \cdot \mathbf{n}_i$ where \mathbf{n}_i is the unit outward normal at control point i .

11. For each control point, the sum of the induced normal velocities has to be equal and opposite to the normal component of the free-stream velocity, $\mathbf{U}_\infty = (u_\infty, w_\infty)$: $\text{RHS}_i = -(u_\infty, w_\infty) \cdot \mathbf{n}_i$

12. So far there are N equations but $N+1$ unknowns. The Kutta condition gives closure: $\gamma_1 + \gamma_{N+1} = 0$

13. Finally we have:

'Influence coefficient' matrix

$$\begin{bmatrix} K_{1,1} & K_{1,2} & \dots & K_{1,N+1} \\ K_{2,1} & K_{2,2} & \dots & K_{2,N+1} \\ \vdots & \vdots & \ddots & \vdots \\ K_{N,1} & K_{N,2} & \dots & K_{N,N+1} \\ 1 & 0 & \dots & 1 \end{bmatrix} \begin{bmatrix} \gamma_1 \\ \gamma_2 \\ \vdots \\ \gamma_N \\ \gamma_{N+1} \end{bmatrix} = \begin{bmatrix} -(u_\infty, w_\infty) \cdot \mathbf{n}_1 \\ -(u_\infty, w_\infty) \cdot \mathbf{n}_2 \\ \vdots \\ -(u_\infty, w_\infty) \cdot \mathbf{n}_N \\ 0 \end{bmatrix} \quad \text{which we solve for } \gamma_1, \dots, \gamma_{N+1}.$$

2D Panel Method: direct method – 6

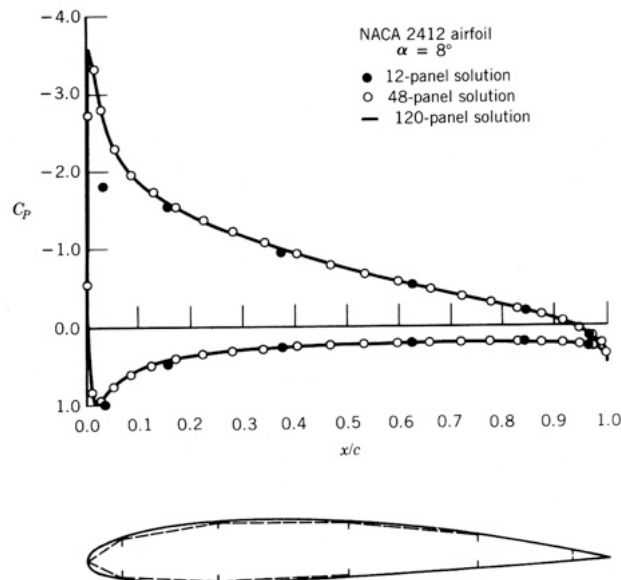
14. Once all the vorticities are known, the tangential velocity at each control point can be found:

$$U_{t,j} = (u_\infty, w_\infty) \cdot \mathbf{t}_j + (\gamma_j + \gamma_{j+1})/4 \quad \text{where } \mathbf{t}_j \text{ is the local panel tangent.}$$

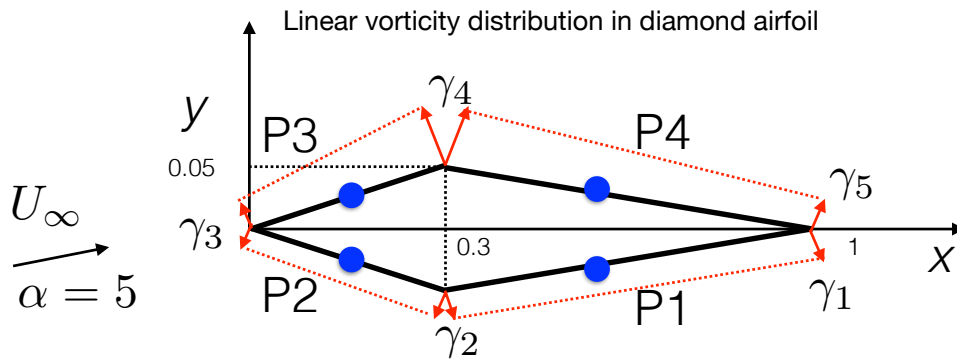
15. From this we can compute the pressure coefficient, contribution to lift, etc:

$$C_{p,j} = 1 - \frac{U_{t,j}^2}{U_\infty^2}; \quad \Delta L_j = \rho U_\infty \frac{\gamma_j + \gamma_{j+1}}{2} \Delta c_j$$

16. The solutions converge as we increase the N , the number of panels:



2D panel method example – 1



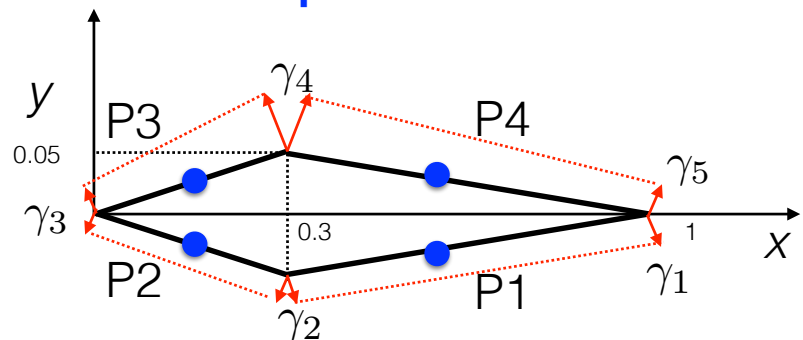
4 panels \rightarrow 5x5 coefficient matrix

panel coordinates	control point	normal vector
(1,0)	(0.65,-0.025)	(0.0712,-0.9975)
(0.3,-0.05)	(0.15,-0.025)	(-0.1644,-0.9864)
(0,0)	(0.15,0.025)	(-0.1644,0.9864)
(0.3,0.05)	(0.65,0.025)	(0.0712,0.9975)
(1,0)		

2D panel method example – 2

Create first row of matrix corresponding to P1
call **vort2dl** to obtain velocities in global coordinates

$(u_a, w_a)_1$
$(u_b, w_b)_1$



(-0.2606, 0.1409)	(0.0015, -0.055)	(-0.0038, -0.0444)	(-0.234, -0.112)	
	(-0.238, -0.1766)	(-0.0004, -0.0448)	(-0.0077, -0.0539)	(-0.2201, 0.1413)

Sum to obtain $(u, v)_{1,j}$

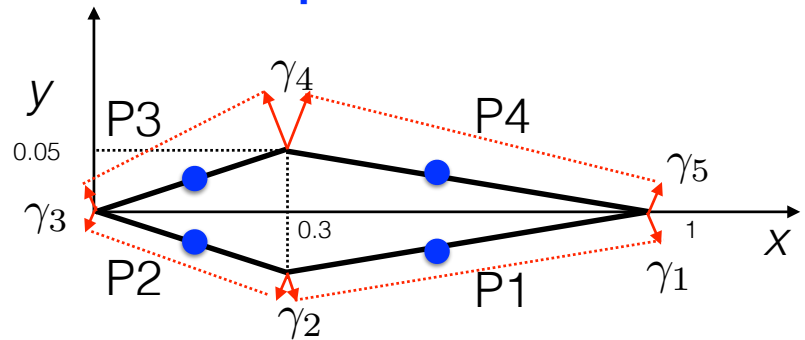
(-0.2606, 0.1409)	(-0.2365, -0.2316)	(-0.00384, -0.0892)	(-0.2347, -0.1659)	(-0.2201, 0.1413)
-------------------	--------------------	---------------------	--------------------	-------------------

Project onto normal vectors $K_{i,j} = (u, v)_{i,j} \cdot \mathbf{n}_i$

$K_{1,j}$	-0.1592	0.2141	0.0887	0.1482	-0.1566
-----------	---------	--------	--------	--------	---------

2D panel method example — 3

Similarly for the next 3 rows



$K_{2,j}$	-0.0988	-0.3339	0.3081	-0.1892	-0.0956
$K_{3,j}$	0.0956	0.1892	-0.3081	0.3339	0.0988
$K_{4,j}$	0.1566	-0.1482	-0.0887	-0.2141	0.1592

Last row of matrix corresponds to Kutta condition $\gamma_1 + \gamma_5 = 0$

$K_{5,j}$	1	0	0	0	1
-----------	---	---	---	---	---

2D panel method example — 4

Assembled influence coefficient matrix

Symmetry properties stem from airfoil symmetry.

$K_{i,j}$	-0.1592	0.2141	0.0887	0.1482	-0.1566
	-0.0988	-0.3339	0.3081	-0.1892	-0.0956
	0.0956	0.1892	-0.3081	0.3339	0.0988
	0.1566	-0.1482	-0.0887	-0.2141	0.1592
	1	0	0	0	1

Generate RHS vector by projecting free stream velocity onto normals $-(U_\infty, W_\infty) \cdot \mathbf{n}_i$

b	0.016	0.2497	0.0778	-0.1579	0
-----	-------	--------	--------	---------	---

Solve linear system $K\gamma = b$

γ	-0.8862	-0.9905	0.4848	1.233	0.8862
----------	---------	---------	--------	-------	--------

Compute velocities in panels $U_{t,j} = (u_\infty, w_\infty) \cdot \mathbf{t}_j + (\gamma_j + \gamma_{j+1})/4$

Compute pressure coefficients and lift $C_{p,j} = 1 - \frac{U_{t,j}^2}{U_\infty^2}; \quad \Delta L_j = \rho U_\infty \frac{\gamma_j + \gamma_{j+1}}{2} \Delta c_j$

$$C_l = 0.53884$$

2D Panel Method: inverse problem

Find the coordinates (x_j, y_j) , $j=1, \dots, N$ of points on the airfoil surface that produce a given distribution of pressure/velocity (i.e. vorticity)

Say we are given the pressure distribution on all panels, $C_{p,j}$. Since the average tangential velocity perturbation on each panel is half its average vorticity (as for thin airfoil theory), we have, for linear vorticity distribution

$$C_{p,j} = 1 - \left[\frac{U_\infty \cos(\alpha + \alpha_j) + 0.25(\gamma_j + \gamma_{j+1})}{U_\infty} \right]^2; \quad j = 1, \dots, N$$

α_j is the panel
 α relative to
chord line

$$\gamma_1 + \gamma_{N+1} = 0$$

Kutta condition at TE

which could be used to find all the vorticities *provided* we know the α_j s (i.e. the airfoil shape).

However, the influence coefficients K_{ij} are nonlinear functions of the coordinates (x_j, y_j) . The solution requires an iterative procedure.

Method of Kennedy and Marsden, J Aircraft **15** 1978 (fixed point iteration):

The ordinates x_j ; $j=1, \dots, N$ are given, and starting from an initial guess (a 'seed airfoil') $y_j(0)$; $j=1, \dots, N$, the iteration for the y-coordinates is

$$y_j^{(n+1)} = \frac{1}{U_\infty \cos \alpha} \left[\psi_0 + \sum_{j=1}^N K_{ij}^{(n)} \gamma_j \right] + x_j \tan \alpha$$

This is iterated until the coordinates converge.

Boundary layer (BL) modelling

Key ideas of BLs for wing design

1. We are mostly interested in the time-average BL behaviour because we can't afford time-varying computations (DNS and LES) in design.
2. BL PDE equations are simpler than the Navier–Stokes equations from which they derive and are parabolic rather than elliptic in nature. That opens up cheaper computational methods if we know the external flow speed/pressure.
3. BL equations are inherently nonlinear, as opposed to potential flow equations for the attached outer flow, which are much cheaper to solve at required accuracy.
4. BLs both laminar and turbulent have some key self-similarity properties (i.e. dimensionless shape invariance w.r.t. downstream distance) that we often seek to exploit.
5. BLs usually/typically start out laminar at the LE and make transition to turbulence some distance downstream, changing the BL equations from laminar to turbulent types. We have to be able to predict transition and change gears from laminar to turbulent, as we march downstream.
6. Mesh-based (finite difference/volume) methods for solution of BL equations are typically still too expensive for airfoil and wing design in design-office scenarios. That forces adoption of wall-normal-integrated BL approaches, which converts BL PDEs to sets of ODEs. These are the basis for most design-office airfoil BL computations (e.g. in XFOIL).
7. In the end we have to couple up the BL solutions to the outer flow solutions, as the BL growth changes the external flow speed distribution. That coupling is known as viscous–inviscid interaction (VII), which is where we head to after learning how to compute BLs.

Analysis of boundary layers – time-average

1. Introduction to BLs: laminar and turbulent flows, transition.
2. BL analysis: simplifying assumptions, formulation and solution methods.
 - i) differential form
 - ii) integral form

In the flow past an airfoil, viscous effects are mainly confined to a thin layer close to the surface of the airfoil (the *boundary layer*) and its wake.

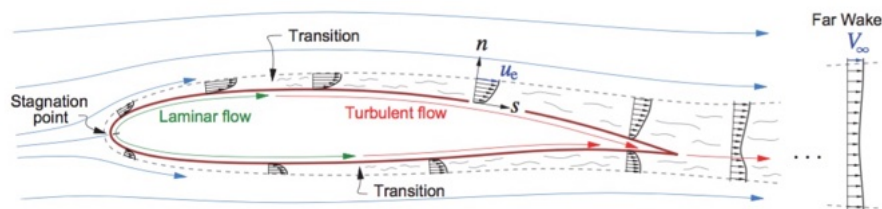


Figure 4.1: Boundary layer and wake development on a typical airfoil, shown by the $u(n)$ velocity profiles. The layer thicknesses are shown exaggerated.

Two important points about BL pressure

1. External to the BL, the flow is effectively inviscid and we can use Bernoulli's equation.

In streamline (s) coordinates external to airfoil, $p_\infty + \frac{1}{2}\rho V_\infty^2 = p(s) + \frac{1}{2}\rho u_e^2(s) = \text{const.}$

$$-\frac{dp}{ds} = \rho u_e \frac{du_e}{ds}$$

2. Since airfoil boundary layers are typically very thin in relation to their radius of curvature

$$\frac{\partial p}{\partial n} \approx 0$$

i.e. BL pressure is that in the external inviscid flow just outside BL, related to flow speed gradient, and constant in wall-normal direction.

Boundary layer modelling: PDE form

For 2D steady/time-average incompressible flow, with $u \sim U_e$, $p \sim \rho U_e^2$, $s \sim c$, $n \sim \delta$
 assuming $\delta \ll c$, $Re \gg 1$, then $\partial/\partial n \gg \partial/\partial s$ and the N-S equations simplify to 'BL equations':

$$\begin{aligned} \frac{\partial u}{\partial s} + \frac{\partial v}{\partial n} &= 0 \\ \rho \left(u \frac{\partial u}{\partial s} + v \frac{\partial u}{\partial n} \right) &= -\frac{\partial p}{\partial s} + \frac{\partial \tau_{ss}}{\partial s} + \frac{\partial \tau_{sn}}{\partial n} \\ \rho \left(u \frac{\partial v}{\partial s} + v \frac{\partial v}{\partial n} \right) &= -\frac{\partial p}{\partial n} + \frac{\partial \tau_{ns}}{\partial s} + \frac{\partial \tau_{nn}}{\partial n} \end{aligned} \Rightarrow \begin{aligned} \frac{\partial u}{\partial s} + \frac{\partial v}{\partial n} &= 0 \\ u \frac{\partial u}{\partial s} + v \frac{\partial u}{\partial n} &= U_e \frac{\partial U_e}{\partial s} + \frac{1}{\rho} \frac{\partial \tau}{\partial n} \\ \frac{\partial p}{\partial n} &= 0 \end{aligned}$$

Important: unlike the NSE and potential flows, which generate elliptic PDEs, the BL equations are 'parabolic' PDEs and are integrated/marched forward in s , given an inlet/LE BC. Also, we must be given U_e in advance.

Laminar flow $\tau = \mu \frac{\partial u}{\partial n}$ so that $\frac{1}{\rho} \frac{\partial \tau}{\partial n} = \nu \frac{\partial^2 u}{\partial n^2}$

Turbulent flow $\tau = \mu \frac{\partial u}{\partial n} - \rho \overline{u'v'}$ and we need a model for the Reynolds stress $\overline{u'v'}$
We will revisit this point in a few slides along.

For the laminar case, assuming the two terms on the RHS of the momentum equation scale like (\sim)

$$U_e \frac{\partial U_e}{\partial s} \sim \frac{U_e^2}{s} \quad \text{and} \quad \frac{1}{\rho} \frac{\partial \tau}{\partial n} = \nu \frac{\partial^2 u}{\partial n^2} \sim \nu \frac{U_e}{\delta^2} \quad \text{and are of similar magnitude: } \frac{U_e^2}{s} \sim \nu \frac{U_e}{\delta^2}$$

we obtain $\delta \sim \sqrt{\frac{s\nu}{U_e}} = \frac{s}{\sqrt{Re_s}} \quad \text{or} \quad \frac{\delta}{s} \sim \frac{1}{\sqrt{Re_s}}$

Finite differences (FD) solution of the BL equations

We note that in principle, solutions to both laminar and turbulent mean-flow BL PDEs can be approximated numerically using grid-based methods (e.g. finite differences). (In practice this is rarely done owing to expense of calculation.)

Reminder: since the BL PDEs are parabolic in nature, they can be 'marched' downstream, starting from initial upstream data.

Here is a simple method that employs forward differences in x and central differences in y :

PDEs:

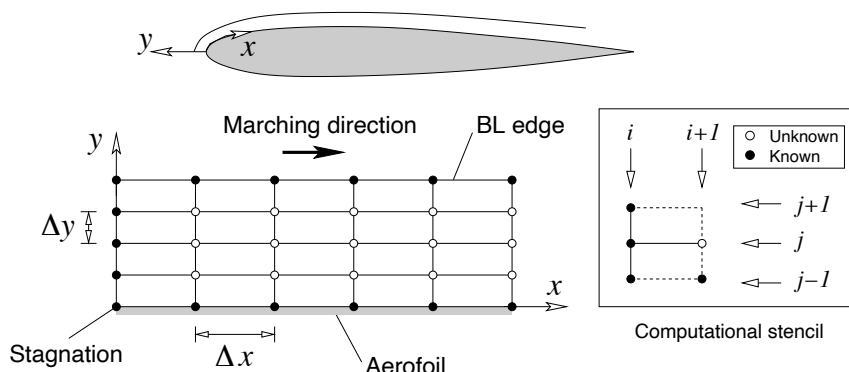
$$u \frac{\partial u}{\partial x} + v \frac{\partial u}{\partial y} = \frac{1}{2} \frac{dU_e^2}{dx} + \nu \frac{\partial^2 u}{\partial y^2} \rightarrow u_{i,j} \frac{u_{i+1,j} - u_{i,j}}{\Delta x} + v_{i,j} \frac{u_{i,j+1} - u_{i,j-1}}{2\Delta y} = \frac{U_e^2|_{i+1} - U_e^2|_i}{2\Delta x} + \nu \frac{u_{i,j+1} - 2u_{i,j} + u_{i,j-1}}{\Delta y^2}$$

FDEs:

$$\frac{\partial u}{\partial x} + \frac{\partial v}{\partial y} = 0 \rightarrow \frac{u_{i+1,j} - u_{i,j}}{\Delta x} + \frac{v_{i+1,j} - v_{i+1,j-1}}{\Delta y} = 0$$

A single streamwise step consists of:

1. March this in x to obtain $u_{i+1,j}$ from $u_{i,j}$.
2. March this in y to obtain $v_{i+1,j}$ from $v_{i+1,j-1}$.



FD: difficulties

1. Requires a (good) solution at the inflow to be known (e.g. Hiemenz stagnation flow)
2. Stability: this particular FD approximation is explicit and for stability requires

$$\Delta x < \frac{u_{\min} \Delta y^2}{2\nu} \quad \text{and} \quad \Delta y < \frac{2\nu}{|v_{\max}|}$$

Problem: u_{\min} approaches zero near the wall and this imposes severe restrictions in the size Δx . Reducing Δx increases the cost.

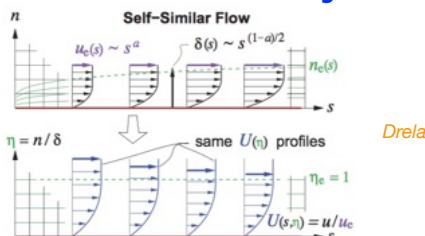
Solution: use an implicit method, more complicated, but stable.

3. The location of the BL edge (largest δ) must be known (or guessed) for mesh design
4. Unsuitable for separated flow: recirculation does not allow for a marching direction

In practice, wall-normal integrated forms of the BL equations (which produces ODEs from PDEs) are typically used for modelling aeronautical BL flows, instead of discretising the BL PDEs and solving them on a grid of points. The wall-normal integrated forms are what we use in practice.

But first, we visit the idea of self-similar BL solutions, that seek to exploit the idea that the dimensionless SHAPE of the BL profile is either invariant, or just slowly varying in the streamwise direction.

Similarity solutions for laminar BLs— 1



1. Consider the laminar zero-pressure gradient (ZPG) BL (with $U_e = \text{const}$). This is described by

$$\frac{\partial u}{\partial s} + \frac{\partial u}{\partial n} = 0, \quad u \frac{\partial u}{\partial s} + v \frac{\partial u}{\partial n} = \nu \frac{\partial^2 u}{\partial s^2}$$

2. We know from order of magnitude analysis that the BL thickness $\delta \sim (sv/U_e)^{1/2}$. The BL profile does not change shape in the streamwise direction when scaled w.r.t. δ , i.e. $u/U_e = \text{function}(n/\delta)$. Instead of (dimensionless) n/δ we could use $\eta = n(U_e/2vs)^{1/2}$; the '2' for convenience later.

3. Next we introduce the streamfunction $\psi = \int u \, dn|_{s=\text{const}}$ which should increase with δ (i.e. as more fluid is entrained from the freestream into the BL), or equivalently with $s^{1/2}$. We write $\psi = (2\nu U_e s)^{1/2} f(\eta)$ which is the dimensionally correct way of describing it in terms of η . Recall that with $u = \partial\psi/\partial n$ and $v = -\partial\psi/\partial s$ the flow will be incompressible. The velocity components are:

$$u = \frac{\partial\psi}{\partial n} = U_e f(\eta), \quad v = -\frac{\partial\psi}{\partial s} = \left(\frac{\nu U_e}{2s}\right)^{1/2} (\eta f' - f) \quad (f' \equiv df/d\eta)$$

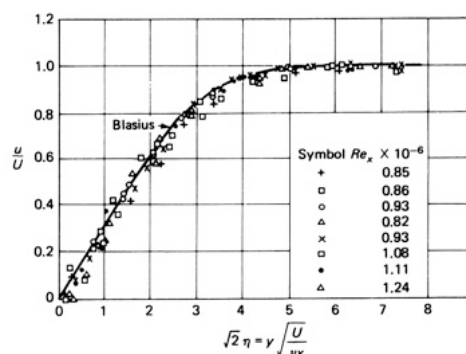
4. Upon substituting these forms into the momentum equation **Blasius (1908)** obtained

$$f''' + f f'' = 0$$

which we note is now an ODE rather than a PDE. The equation is solved subject to the BCs

$$f'(0) = f(0) = 0, \quad f'(\infty) = 1$$

The (numerical) solution to this equation agrees well with experimental results.



White

Similarity solutions for laminar BLs – 2

5. **Faulkner and Skan (1931)** showed that Blasius' similarity solution can be generalized if the freestream velocity U_e is a power-law function of s , i.e. $U_e(s) = Ks^m$ in which case the similarity variable $\eta = Cns^a$ with $m = 2a + 1$. Blasius' ZPG solution is the special case for $m = 0$.

The external pressure gradient is required to be $\frac{dp}{ds} = -\rho U_e^2 \frac{m}{s}$

6. The similarity variable η now contains the exponent m : $\eta = y \left(\frac{m+1}{2} \frac{U_e}{\nu s} \right)^{1/2}$

7. The result corresponding to Blasius' ODE is the Falkner–Skan equation

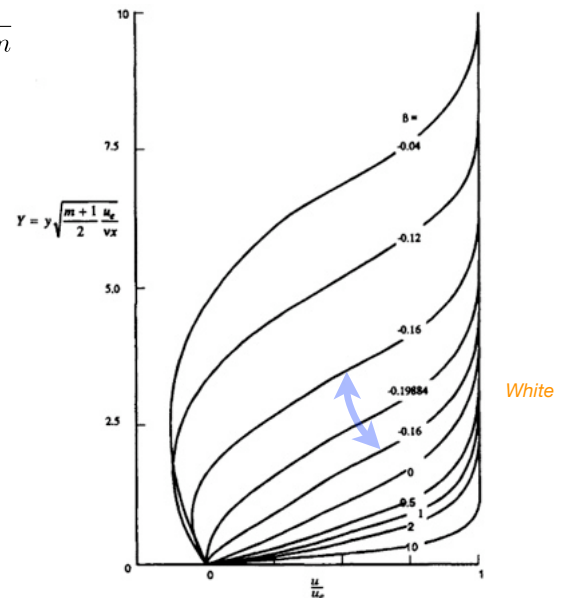
$$f''' + ff'' + \beta(1 - f^2) = 0, \quad \text{where} \quad \beta = \frac{2m}{1+m}$$

BCs are as before: $f'(0) = f(0) = 0, \quad f'(\infty) = 1$

8. The equation is solved numerically. Stewartson (1954) pointed out that for $\beta < 0$ there are a number of solution branches, some of which provide reversed flow near the wall (see e.g. two different solution curves for $\beta = -0.16$).

Incipient flow separation corresponds to $\beta = -0.19884$, while Blasius' solution corresponds to $\beta = 0$.

A key point is that we have generalised the (Blasius) similarity solution for the zero-pressure-gradient BL, giving self-similar/equilibrium BL shapes as a function of pressure gradient and local skin friction coefficient.



Modelling of turbulent BLs

1. Turbulent flow is chaotic/random, complicated, and varies in both space and time. Unlike some laminar flows (e.g. Blasius BL), turbulent flows cannot be solved in closed form.

2. Analyzing/modelling turbulent flows for engineering design is based in statistics and turbulence models that attempt to model fluctuating quantities in terms of their mean values.

3. BL turbulence (i.e. in attached BL flow) is somewhat easier to deal with than the general case.

4. Propose that any quantity can be decomposed into a mean value and a zero-mean fluctuation:

$$u = \bar{u} + u' \quad \bar{u} = \frac{1}{T} \int_0^T u \, dt \quad \text{The mean of a product: } \overline{uv} = \overline{(\bar{u} + u')(\bar{v} + v')} = \bar{u}\bar{v} + \overline{u'v'}$$

5. Noting that with the incompressibility constraint $\frac{\partial u}{\partial s} + \frac{\partial v}{\partial n} = 0$ we have

6. Now we can write the time-mean BL momentum equation as $u \frac{\partial u}{\partial s} + v \frac{\partial u}{\partial n} \equiv \frac{\partial uu}{\partial s} + \frac{\partial uv}{\partial n}$

$$\frac{\partial \overline{uu}}{\partial s} + \frac{\partial \overline{uv}}{\partial n} = U_e \frac{\partial U_e}{\partial s} + \frac{\mu}{\rho} \frac{\partial^2 \bar{u}}{\partial n^2} \rightarrow \bar{u} \frac{\partial \bar{u}}{\partial s} + \bar{v} \frac{\partial \bar{u}}{\partial n} = U_e \frac{\partial U_e}{\partial s} + \frac{\mu}{\rho} \frac{\partial^2 \bar{u}}{\partial n^2} - \frac{\partial \overline{u'v'}}{\partial n}$$

7. The quantity $\rho \overline{u'v'}$ is called a Reynolds stress in honour of Osborne Reynolds.

8. Trouble: the equation set is no longer closed because we introduced this new variable. The task of a turbulence model is to guess a relationship between the Reynolds stresses and the mean velocities, thus closing the set of equations.

9. The simplest workable approach is the mixing length model (due to Prandtl): $-\overline{u'v'} = l_{\text{mix}} \left| \frac{\partial \bar{u}}{\partial n} \right| \frac{\partial \bar{u}}{\partial n}$

10. For a turbulent BL, $l_{\text{mix}} = \kappa n$ where $\kappa \approx 0.4$ is the von Karman constant.

In this case we have $\tau(s, n) = \tau_l + \tau_t = (\mu + \mu_t(s, n)) \frac{\partial u}{\partial n}$

Laminar vs turbulent BL

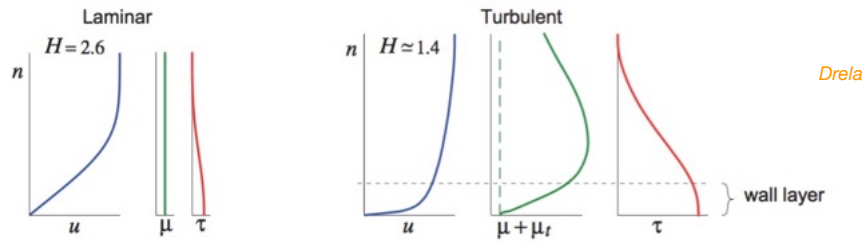
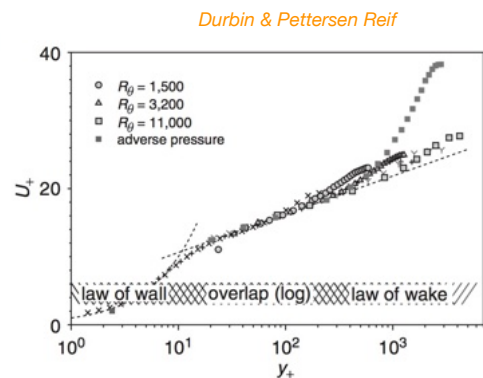


Figure 4.5: Comparison of laminar and turbulent flat-plate velocity, viscosity, and shear profiles. The shape parameter H is introduced in Section 4.5.

The key feature which makes turbulent boundary layers so different is that μ_t is large relative to μ over most of the turbulent boundary layer, but falls linearly to zero over roughly the bottom 20% portion called the *wall layer*. Here the total stress τ is approximately constant and equal to the wall shear stress τ_w . Hence in the wall layer $\partial u / \partial n$ varies roughly as $1/n$, and therefore $u(n) \sim \ln n$. The variation of all the quantities in the wall layer can be summarized as follows.

$$\begin{aligned} \tau(n) &\simeq \tau_w \sim \text{const.} \\ \mu_t(n) &\sim n \\ \partial u / \partial n &= \tau(n) / \mu_t(n) \sim 1/n \quad (\text{assuming } \mu \ll \mu_t) \\ u(n) &\sim \ln n \end{aligned}$$

This is a robust feature of equilibrium turbulent boundary layer profiles: they have logarithmic shape over some portion (close to the wall, but not at the wall). True for all kinds of external pressure gradients (see e.g. Coles 1956).

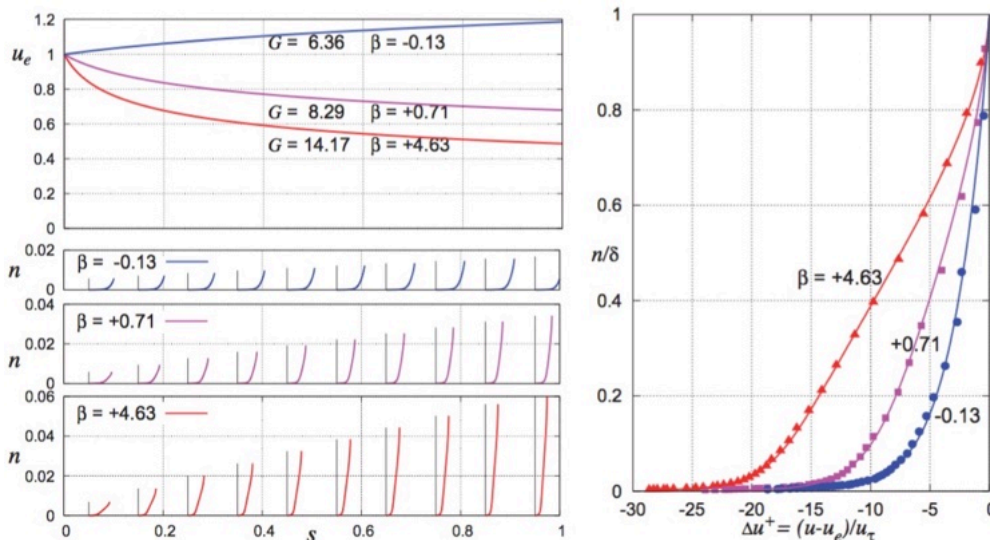


Self-similar turbulent BLs

Just like laminar BLs with carefully controlled external pressure gradients, turbulent BLs can take self-similar (a.k.a. equilibrium) shapes for zero, adverse and favourable pressure gradients of suitable streamwise variation (Clauser 1954).

In this case the appropriate form of the dimensionless velocity profile is the velocity defect normalised by the 'friction velocity' which is a measure of the wall shear traction τ_w . We plot

$$\Delta u^+ = \frac{u(s, n) - U_e(s)}{u_\tau} \quad \text{where} \quad u_\tau = \sqrt{\frac{\tau_w}{\rho}} \quad \text{vs} \quad \eta(s, n) = \frac{n}{\delta(s)}$$



β and G are parameters of the self-similar shape, pressure gradient, skin friction.

$\beta = 0$ gives the standard ZPG turbulent BL.

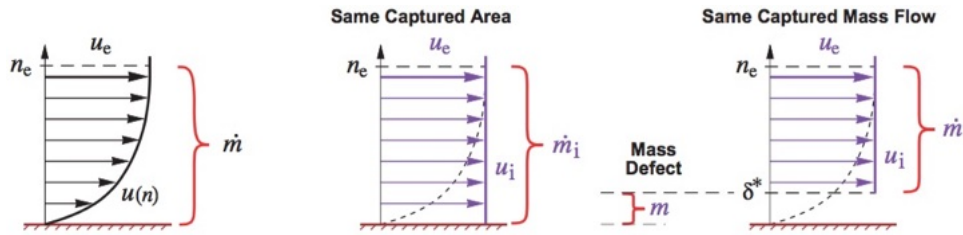
$\beta > 0$ corresponds to an adverse pressure gradient while $\beta < 0$ corresponds to a favourable gradient.

$$\Delta u^+(0) = -\sqrt{\frac{2}{c_f}}$$

Defect integrals and thicknesses

In the following, u_i is the inviscid external inviscid flow speed u_e carried down to the wall.
And n_e is the wall-normal distance to the edge of the BL.

Mass flow comparison between the true viscous flow and the “equivalent inviscid flow”



Drela

mass flow rate per unit span $\dot{m} = \int d\dot{m} = \int_0^{n_e} \rho u \, dn = \int_0^{n_e} \rho_e u_e \, dn - \int_0^{n_e} (\rho_e u_e - \rho u) \, dn$

or $\dot{m} = \dot{m}_i - m$

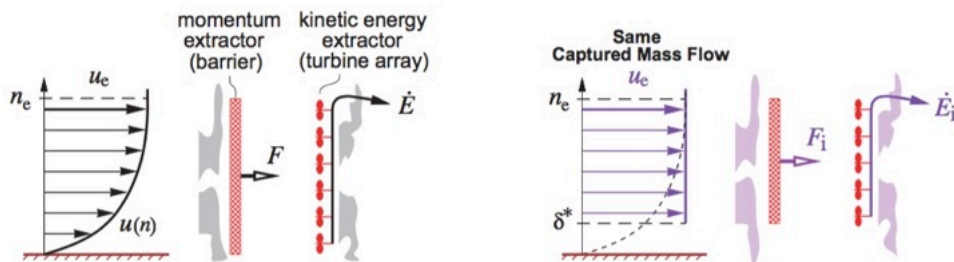
where $\dot{m}_i \equiv \int_0^{n_e} \rho_e u_e \, dn = \rho_e u_e n_e$

$m \equiv \int_0^{n_e} (\rho_e u_e - \rho u) \, dn = \rho_e u_e \delta^*$ mass flow defect

and $\delta^* \equiv \int_0^{n_e} \left(1 - \frac{\rho u}{\rho_e u_e}\right) \, dn$ displacement thickness

Defect integrals and thicknesses

Momentum and kinetic energy flow (force and power) comparisons



Drela

Figure 4.3: Comparison of actual and EIF's momentum flow and kinetic energy flow, for the same mass flow. Momentum flow is equal to the force on a hypothetical barrier which brings the fluid stream's s -velocity to zero. Kinetic energy flow is equal to the power from an ideal turbine array which brings the fluid stream's velocity to zero reversibly.

momentum flow
per unit span

$$F = \int u \, d\dot{m} = \int_0^{n_e} \rho u^2 \, dn = \int_0^{n_e} \rho_e u_e^2 \, dn - u_e \int_0^{n_e} (\rho_e u_e - \rho u) \, dn - \int_0^{n_e} (u_e - u) \rho u \, dn$$

$$= \rho_e u_e^2 n_e - u_e (\rho_e u_e \delta^*) - \rho_e u_e^2 \theta$$

$$F = F_i - P \quad (4.7)$$

energy flow per unit
span

$$\dot{E} = \int \frac{1}{2} u^2 \, d\dot{m} = \int_0^{n_e} \frac{1}{2} \rho u^3 \, dn = \int_0^{n_e} \frac{1}{2} \rho_e u_e^3 \, dn - \frac{1}{2} u_e^2 \int_0^{n_e} (\rho_e u_e - \rho u) \, dn - \int_0^{n_e} \frac{1}{2} (u_e^2 - u^2) \rho u \, dn$$

$$= \frac{1}{2} \rho_e u_e^3 n_e - \frac{1}{2} u_e^2 (\rho_e u_e \delta^*) - \frac{1}{2} \rho_e u_e^3 \theta^*$$

$$\dot{E} = \dot{E}_i - K \quad (4.8)$$

Defect integrals and thicknesses

Integral defects and associated thicknesses

$$\begin{aligned}
 P &\equiv \int_0^{n_e} (u_e - u) \rho u \, dn = \rho_e u_e^2 \theta && \text{(momentum defect)} \\
 K &\equiv \int_0^{n_e} \frac{1}{2} (u_e^2 - u^2) \rho u \, dn = \frac{1}{2} \rho_e u_e^3 \theta^* && \text{(kinetic energy defect)} \\
 \theta &\equiv \int_0^{n_e} \left(1 - \frac{u}{u_e}\right) \frac{\rho u}{\rho_e u_e} \, dn && \text{(momentum thickness)} \\
 \theta^* &\equiv \int_0^{n_e} \left(1 - \frac{u^2}{u_e^2}\right) \frac{\rho u}{\rho_e u_e} \, dn && \text{(kinetic energy thickness)}
 \end{aligned}$$

For incompressible flows, the thickness quantities are just functions of BL shape. If $\rho_e = \rho$:

$$U \equiv \frac{u}{u_e}$$

$$\delta^* = \int_0^{n_e} (1 - U) \, dn, \quad \theta = \int_0^{n_e} (U - U^2) \, dn, \quad \theta^* = \int_0^{n_e} (U - U^3) \, dn$$

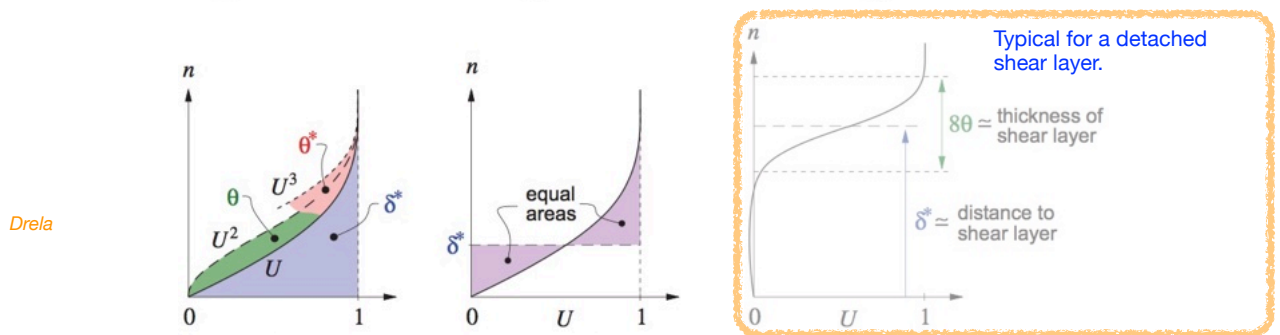


Figure 4.4: Interpretation of the integral thicknesses for incompressible flow, in terms of the geometry of the normalized velocity profile $U = u/u_e$, and also U^2 and U^3 . Since the horizontal scale is dimensionless, the areas have the same length unit as the vertical n axis.

Boundary layer equations

Using the thin shear layer TSL approximations

$$\begin{aligned}
 v &\ll u \\
 \frac{\partial u}{\partial s} &\ll \frac{\partial u}{\partial n} && \text{leads to} \\
 \frac{\partial p}{\partial n} &\simeq 0
 \end{aligned}
 \quad \bar{\tau} = \begin{bmatrix} \tau_{ss} & \tau_{sn} \\ \tau_{ns} & \tau_{nn} \end{bmatrix} \simeq \begin{bmatrix} 0 & \tau \\ \tau & 0 \end{bmatrix}$$

and the boundary layer equations

$$\text{recall } -\frac{\partial p}{\partial s} \approx \rho_e u_e \frac{du_e}{ds}$$

$$\begin{aligned}
 \frac{\partial \rho u}{\partial s} + \frac{\partial \rho v}{\partial n} &= 0 \\
 \rho u \frac{\partial u}{\partial s} + \rho v \frac{\partial u}{\partial n} &= \rho_e u_e \frac{du_e}{ds} + \frac{\partial \tau}{\partial n} \\
 \tau &= (\mu + \mu_t) \frac{\partial u}{\partial n}
 \end{aligned}$$

continuity

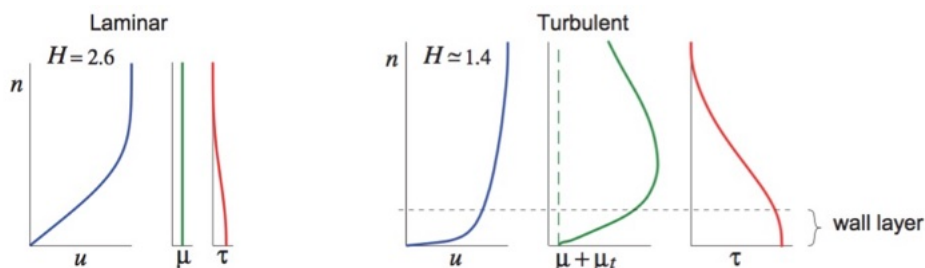
s-component momentum

(this form for turbulent shear stress is an approximation only)

with boundary conditions

$$\begin{aligned}
 \text{at wall, } n=0 : & \quad u=0, \quad v=0 \\
 \text{at edge, } n=n_e : & \quad u=u_e
 \end{aligned}$$

recall



$$H = \frac{\delta^*}{\theta} > 1$$

Drela

Figure 4.5: Comparison of laminar and turbulent flat-plate velocity, viscosity, and shear profiles.

BL response to pressure and shear gradients

Response to streamwise pressure gradients

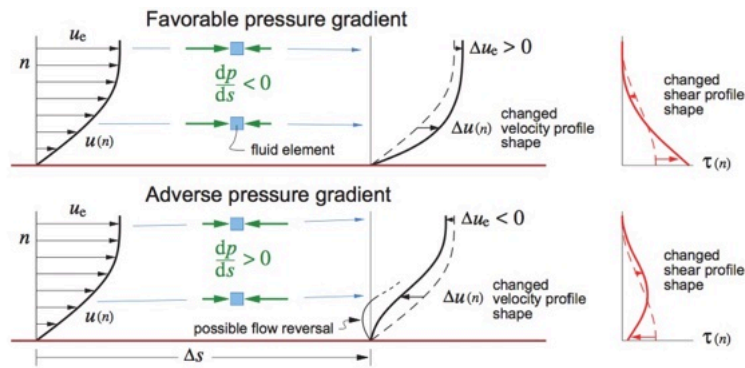


Figure 4.6: Velocity changes Δu along streamlines resulting from a favorable or adverse pressure gradient which applies the same accelerating or decelerating net force per unit volume to all fluid elements. Slower-moving elements have a larger Δu , resulting a distortion of the velocity profile. A sufficiently strong adverse pressure gradient will cause a flow reversal and boundary layer separation.

Response to wall-normal shear gradient

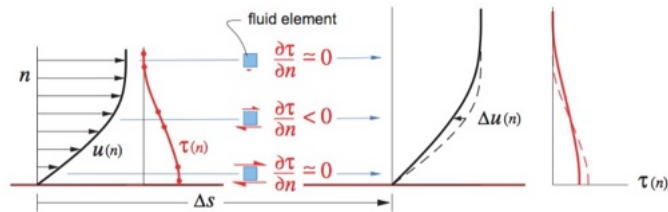


Figure 4.7: A transverse shear gradient produces a net streamwise force per unit volume which tends to "flatten" the velocity profile, and results in an overall growth of the boundary layer.

(Wall-normal) Integral BL relations – 1

The integral momentum analysis begins by combining the continuity and s -momentum equations as follows.

$$\begin{aligned} (u_e - u) \left[\frac{\partial \rho u}{\partial s} + \frac{\partial \rho v}{\partial n} = 0 \right] \\ - \left[\rho u \frac{\partial u}{\partial s} + \rho v \frac{\partial u}{\partial n} = \rho_e u_e \frac{du_e}{ds} + \frac{\partial \tau}{\partial n} \right] \\ \frac{\partial}{\partial s} [(u_e - u) \rho u] + \frac{\partial}{\partial n} [(u_e - u) \rho v] = -(\rho_e u_e - \rho u) \frac{du_e}{ds} - \frac{\partial \tau}{\partial n} \end{aligned} \quad (4.25)$$

Integrating $\int_0^{n_e} [\text{equation (4.25)}] dn$ term by term then gives the dimensional form of the **von Karman integral momentum equation**,

$$\frac{d}{ds} (\rho_e u_e^2 \theta) = \tau_w - \rho_e u_e \delta^* \frac{du_e}{ds} \quad (4.26)$$

(recall momentum defect P): or equivalently $\frac{dP}{ds} = \tau_w + \delta^* \frac{dP}{ds} \quad (4.27)$

Dimensionless form: $\frac{d\theta}{ds} = \frac{c_f}{2} - (H + 2 - M_e^2) \frac{\theta}{u_e} \frac{du_e}{ds}$ where $H \equiv \frac{\delta^*}{\theta}$ shape parameter
 $c_f \equiv \frac{\tau_w}{\frac{1}{2} \rho_e u_e^2}$ skin friction coefficient
 $M_e \equiv \frac{u_e}{a_e}$ edge Mach number

Incompressible flow:

$$\frac{d\theta}{ds} = \frac{c_f}{2} - (H + 2) \frac{\theta}{u_e} \frac{du_e}{ds} \equiv \frac{c_f}{2} - \frac{\delta^* + 2\theta}{u_e} \frac{du_e}{ds}$$

Potentially we could integrate this in s using θ to get u_e or vice-versa, given $c_f \dots$

(Wall-normal) Integral BL relations – 2

An equation for the **kinetic energy** is obtained by multiplying the momentum equation by the velocity u . The mass equation is also incorporated to put the result into divergence form as follows.

$$\begin{aligned} & \frac{1}{2} (u_e^2 - u^2) \left[\frac{\partial \rho u}{\partial s} + \frac{\partial \rho v}{\partial n} = 0 \right] \\ & - u \left[\rho u \frac{\partial u}{\partial s} + \rho v \frac{\partial u}{\partial n} = \rho_e u_e \frac{du_e}{ds} + \frac{\partial \tau}{\partial n} \right] \\ & \frac{\partial}{\partial s} \left[\frac{1}{2} (u_e^2 - u^2) \rho u \right] + \frac{\partial}{\partial n} \left[\frac{1}{2} (u_e^2 - u^2) \rho v \right] = -u(\rho_e - \rho) u_e \frac{du_e}{ds} - u \frac{\partial \tau}{\partial n} \end{aligned} \quad (4.30)$$

Integrating $\int_0^{n_e}$ [equation (4.30)] dn term by term gives the dimensional **integral kinetic energy equation**,

$$\frac{d}{ds} \left(\frac{1}{2} \rho_e u_e^3 \theta^* \right) = \mathcal{D} - \rho_e u_e^2 \delta^{**} \frac{du_e}{ds} \quad (4.31)$$

(recall kinetic energy defect K): or equivalently $\frac{dK}{ds} = \mathcal{D} + u_e \delta^{**} \frac{dp}{ds}$ (4.32)

where

$$\delta^{**} \equiv \int_0^{n_e} \left(1 - \frac{\rho}{\rho_e} \right) \frac{u}{u_e} dn \quad \text{density flux thickness (} = 0 \text{ for incompressible flow)}$$

$$\mathcal{D} \equiv \int_0^{n_e} \tau \frac{\partial u}{\partial n} dn = \int_0^{n_e} (\mu + \mu_t) \left(\frac{\partial u}{\partial n} \right)^2 dn \quad \text{dissipation integral}$$

Dimensionless form:

$$\frac{d\theta^*}{ds} = 2c_D - \left(\frac{2H^{**}}{H^*} + 3 - M_e^2 \right) \frac{\theta^*}{u_e} \frac{du_e}{ds} \quad \begin{aligned} H^* &\equiv \frac{\theta^*}{\theta} && \text{kinetic energy shape parameter} \\ H^{**} &\equiv \frac{\delta^{**}}{\theta} && \text{density flux shape parameter} \\ c_D &\equiv \frac{\mathcal{D}}{\rho_e u_e^3} && \text{dissipation coefficient} \end{aligned}$$

Incompressible flow:

$$\frac{d\theta^*}{ds} = 2c_D - 3 \frac{\theta^*}{u_e} \frac{du_e}{ds}$$

Integral defect evolution

Momentum defect

$$\begin{aligned} \int_0^s \left\{ \frac{dP}{ds'} \right\} ds' &= \tau_w - m \frac{du_e}{ds'} \Big|_0^s \\ P(s) &= \int_0^s \tau_w ds' + \int_0^s -m \frac{du_e}{ds'} ds' \quad (\text{on airfoil surface}) \\ P(s) &= P_{TE} + \int_{s_{TE}}^s -m \frac{du_e}{ds'} ds' \quad (\text{in wake}) \end{aligned}$$

Kinetic energy defect

$$\begin{aligned} \int_0^s \left\{ \frac{dK}{ds'} \right\} ds' &= \mathcal{D} \Big|_0^s \\ K(s) &= \int_0^s \mathcal{D} ds' \quad (\text{on airfoil surface}) \\ K(s) &= K_{TE} + \int_{s_{TE}}^s \mathcal{D} ds' \quad (\text{in wake}) \end{aligned}$$

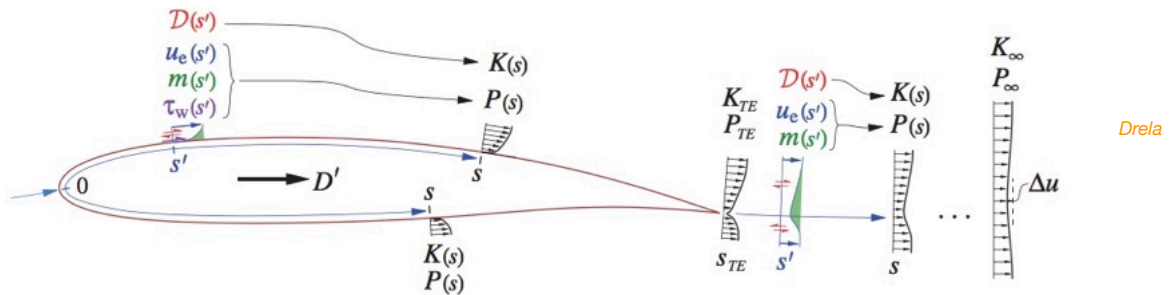
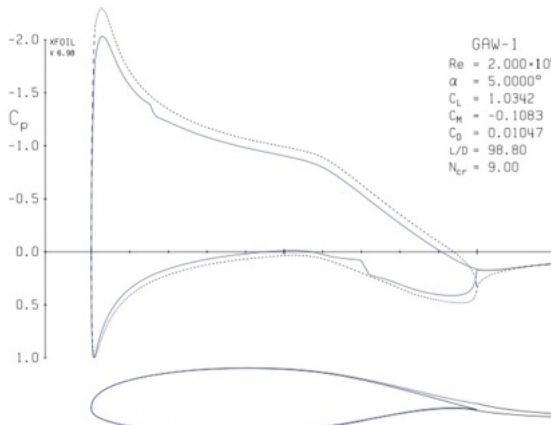


Figure 4.8: Momentum defect $P(s)$ at any location s , including in the wake, obtained as an integral over upstream $\tau_w, m, u_e(s')$ distributions. Kinetic energy defect $K(s)$ is obtained from upstream $\mathcal{D}(s')$ distribution. Far-downstream wake's P_∞, K_∞ are related to the airfoil's profile drag/span D' .

Integral defect evolution, contribution to drag



Drag force per unit span D'

$$D' = P_\infty = \int_{\text{airfoil}} \tau_w ds + \int_{\text{airfoil+wake}} -m \frac{du_e}{ds} ds$$

and since

$$K_\infty = P_\infty V_\infty$$

Drag power per unit span $D'V_\infty$

$$D'V_\infty = K_\infty = \int_{\text{airfoil+wake}} \mathcal{D} ds$$

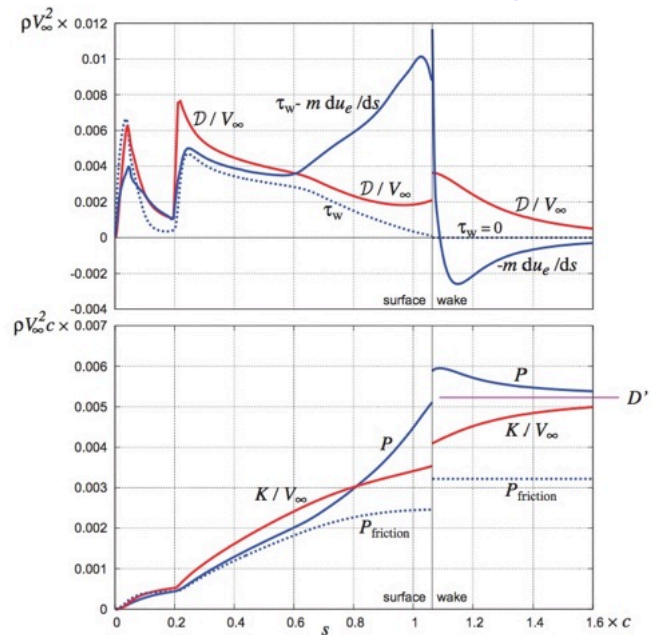


Figure 4.10: Distributions of boundary layer parameters for upper surface and wake of GAW-1 airfoil at $\alpha = 5^\circ$, $Re = 2 \times 10^6$. Transition occurs at $s \approx 0.2c$, where τ_w and \mathcal{D} increase sharply. P and K/V_∞ in the far wake asymptote towards the profile drag/span D' . The jumps in P and K at the trailing edge are from the bottom surface's P and K (not shown) adding to the wake.

Simple BL modelling: integral form — 1

1. Integral-type approaches are comparatively simple and were the first successful methods for general boundary-layer flows. They are based on wall-normal integration of the BL momentum equations, as originally proposed by von Karman in 1921. (Converts PDE into ODE.)
2. It is helpful to have integral measures of boundary-layer shape. The two most useful ones are the boundary layer displacement thickness δ^* and momentum thickness θ .

δ^* : thickness of a layer of zero velocity producing the same volume-flow deficit as the BL

θ : thickness of a layer of zero velocity producing the same momentum deficit as the BL.

Their ratio $H = \delta^*/\theta > 1$ is a useful dimensionless parameter of BL shape.

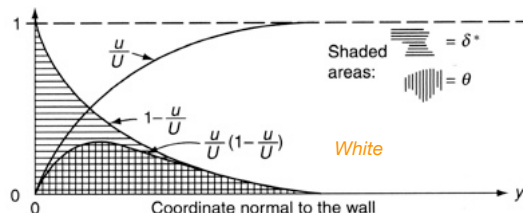
$$H = 2.59 \quad (\text{Blasius BL})$$

$$2.3 \lesssim H \lesssim 3.5 \quad \text{Laminar BL}$$

$$1.3 \lesssim H \lesssim 2.2 \quad \text{Turbulent BL}$$

$$\delta^* = \int_0^\infty \left(1 - \frac{u}{U_e}\right) dy$$

$$\theta = \int_0^\infty \frac{u}{U_e} \left(1 - \frac{u}{U_e}\right) dy$$



$$c_f = \frac{\tau_w}{\frac{1}{2} \rho U_e^2} = 2 \frac{d\theta}{ds} \quad \text{for zero pressure gradient}$$

$$H = \frac{\delta^*}{\theta} > 1$$

3. Start with the BL equations

$$\frac{\partial u}{\partial x} + \frac{\partial v}{\partial y} = 0 \quad \text{continuity}$$

$$u \frac{\partial u}{\partial x} + v \frac{\partial u}{\partial y} = U_e \frac{\partial U_e}{\partial x} + \frac{1}{\rho} \frac{\partial \tau}{\partial y} \quad \text{momentum}$$

4. Subtract $(u - U_e) \times$ continuity from momentum to get

$$-\frac{1}{\rho} \frac{\partial \tau}{\partial y} = \frac{\partial}{\partial x} (u U_e - u^2) + (U_e - u) \frac{\partial U_e}{\partial x} + \frac{\partial}{\partial y} (v U_e - v u)$$

Simple BL modelling: integral form – 2

5. Now integrate to ∞ in y direction, note that $\tau_w=0$ and allow a *transpiration velocity* v_w :

$$\frac{\tau_w}{\rho} = \frac{d}{dx} \int_0^\infty u(U_e - u) dy + \frac{dU_e}{dx} \int_0^\infty (U_e - u) dy - U_e v_w$$

This is useful in later developments.

6. Substitute in the measures δ^* and θ , rearrange:

$$\frac{\tau_w}{\rho U_e^2} = \frac{C_f}{2} = \frac{d\theta}{dx} + (2\theta + \delta^*) \frac{1}{U_e} \frac{dU_e}{dx} - \frac{v_w}{U_e}$$

or, with transpiration velocity $v_w=0$ and some more rearrangement:

$$\frac{C_f}{2} = \frac{d\theta}{dx} + (2 + H) \frac{\theta}{U_e} \frac{dU_e}{dx}$$

Have converted a PDE to an ODE by integrating in one direction.

Given $U_e(x)$ and information about BL shapes, we can integrate this to obtain $C_f(x)$.

7. Two general classes of methods solve this integral BL momentum equation

i): assume a form of BL shape

ii): use empirical correlations between the integral parameters θ and H

A standard shared assumption is that

$$u(x, y) \approx U_e(x) f[\eta, P(x)] \quad \text{where} \quad \eta = y/\delta \quad \text{and} \quad P(x) \text{ is a dimensionless parameter}$$

Unlike similarity solutions the BL shape can evolve in the streamwise direction.

BL integral method of Polhausen

1. Polhausen's method (1921) is of assumed shape function type, a 4th-order polynomial in $\eta=y/\delta$:

$$\frac{u}{U_e} = a_0 + a_1\eta + a_2\eta^2 + a_3\eta^3 + a_4\eta^4$$

$$\text{BCs for } u(x, \eta): \quad u(x, 0) = 0; \quad u(x, 1) = U_e; \quad \frac{\partial u}{\partial y}(x, 1) = 0; \quad \frac{\partial^2 u}{\partial x^2}(x, 1) = 0$$

$$\text{At the wall, } \eta=0, \quad \nu \frac{\partial^2 u}{\partial y^2} = \frac{1}{\rho} \frac{dp}{dx} = -U_e \frac{dU_e}{dx} \implies \frac{\partial^2 u}{\partial \eta^2} = -\frac{\delta^2}{\nu} U_e \frac{dU_e}{dx} \quad \text{and call} \quad \Lambda = \frac{\delta^2}{\nu} \frac{dU_e}{dx} = \frac{\delta^2 U'}{\nu}$$

2. The BL velocity profile is then

$$\frac{u}{U_e} = 2\eta - 2\eta^3 + \eta^4 + \frac{\Lambda}{6} [\eta(1-\eta)^3]$$

$$\text{with } \delta^* = \delta \left(\frac{3}{10} - \frac{\Lambda}{120} \right); \quad \theta = \frac{\delta}{63} \left(\frac{37}{5} - \frac{\Lambda}{15} - \frac{\Lambda^2}{144} \right)$$

3. Substituting into the momentum integral equation gives

$$\frac{d\theta}{dx} = \frac{F(\Lambda)}{U_e}$$

$$\text{where } F(\Lambda) = 2 \left(\frac{3}{315} - \frac{\Lambda}{945} - \frac{\Lambda^2}{9072} \right) \left(2 - \frac{116\Lambda}{945} + \frac{79\Lambda^2}{7560} + \frac{2\Lambda^3}{9072} \right)$$

4. This ODE is solved by marching in x given an initial θ , e.g. using Runge-Kutta.

Method is simple but inaccurate.

BL integral method of Thwaites — 1

1. Thwaites' method (1949) is of empirical correlation type, built on work by Holstein & Bohlen (1940).

2. Starting with $\frac{C_f}{2} = \frac{d\theta}{dx} + (2+H) \frac{\theta}{U_e} \frac{dU_e}{dx}$ multiply through by (Reynolds number) $U_e \theta / \nu$

$$\frac{\tau_w \theta}{\mu U_e} = \frac{U_e \theta}{\nu} \frac{d\theta}{dx} + \frac{\theta^2 U'_e}{\nu} (2+H)$$

3. It is assumed that the (dimensionless) friction and shape factor H are functions of **one** new parameter

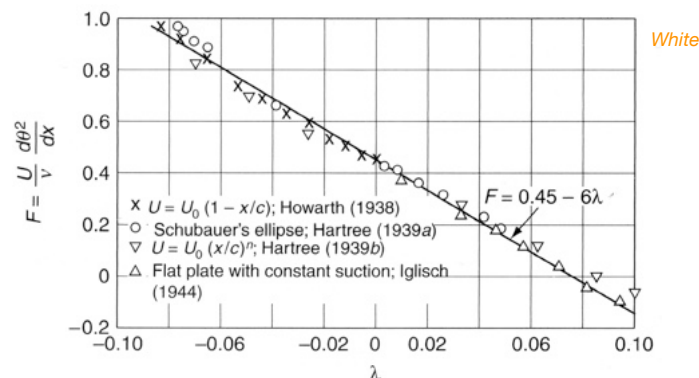
$$\lambda = \frac{\theta^2 U'_e}{\nu} = \left(\frac{\theta}{\delta}\right)^2 \Lambda \quad \text{recall: } \Lambda = \frac{\delta^2}{\nu} \frac{dU_e}{dx} = \frac{\delta^2 U'_e}{\nu} \quad \text{i.e. shear correlation } \frac{\tau_w \theta}{\mu U_e} = S(\lambda)$$

and shape correlation $H = \frac{\delta^*}{\theta} = H(\lambda)$

4. Using $\theta d\theta = \frac{1}{2} d(\theta^2)$ re-arrange the integral BL equation above to give

$$U_e \frac{d}{dx} \left(\frac{\lambda}{U'_e} \right) = 2 \{ S(\lambda) - \lambda [2 + H(\lambda)] \} = F(\lambda)$$

5. Thwaites found that essentially all the available **attached** BL data fit a very simple relationship for $F(\lambda)$:



$$F(\lambda) \approx 0.45 - 6.0\lambda$$

BL integral method of Thwaites — 2

6. When $F(\lambda) = a - b(\lambda)$ the closed-form solution of the modified BL equation is

$$\frac{\theta^2}{\nu} = a U_e^{-b} \left(\int_{x_0}^x U_e^{b-1} dx + C \right)$$

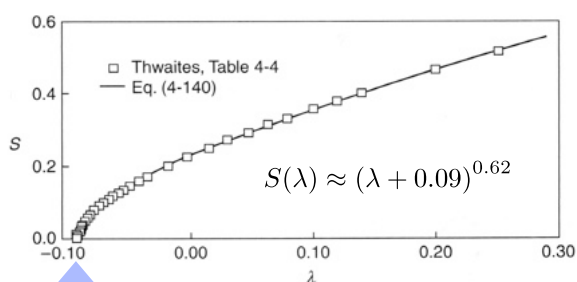
and if x_0 is a stagnation point, $C=0$ is needed to avoid $\theta \rightarrow \infty$ where $U_e=0$.

7. So Thwaites showed that for all types of laminar attached BLs, $\theta(x)$ is well modelled by

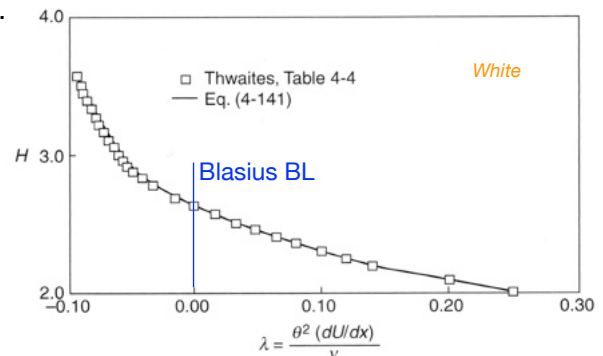
$$\theta^2 \approx \frac{0.45\nu}{U_e^6} \int_0^x U_e^5 dx$$

8. Then calculate $\lambda = \frac{\theta^2 U'_e}{\nu}$; $\tau_w = \frac{\mu U_e}{\theta} S(\lambda)$; $\delta^* = \theta H(\lambda)$

using Thwaites' correlations for $S(\lambda)$ and $H(\lambda)$.



separation when $\lambda = -0.09$



$$H(\lambda) \approx 2.0 + 4.14z - 83.5z^2 + 854z^3 - 3337z^4 + 4576z^5$$

$$z = (0.25 - \lambda)$$

Simple BL modelling: integral form — 3

8. Unfortunately Thwaites method cannot deal with separated flow (which is needed e.g. to integrate through separation bubbles), and Polhausen's method is not very accurate. Neither of them can deal with turbulent flow (or transition). However, the assumed shape function methods (like Polhausen) can be made to work well if more equations are used, and we also use more general shape functions.

To create methods which can deal with flow separation we need to add one more integral equation (for the energy defect) to the von Karman equation. However the methods become rather more involved.

In addition we need models that can deal with the transition from laminar to turbulent flows. This requires a separate set of equations (for perturbation growth in the streamwise direction) that are coupled with the solution of the two integral equations.

Integral BL modelling: 2-equation methods — 1

The methods described so far lack generality: they cannot cope with flow separation and also did not consider turbulent BLs. Now we look at methods which rely on simultaneous solutions of the (incompressible) momentum and kinetic-energy defect integrals. Our development follows Drela and Giles (1987), *AIAA J* **25**(10): 1347–1355, and Drela's MIT OCW notes for Viscous Aerodynamics 16-041, but there is a variety of other related treatments which matured in the 1980s.

$$\frac{d\theta}{ds} + (2 + H) \frac{\theta}{u_e} \frac{du_e}{ds} = \frac{c_f}{2}$$

$$c_f = \frac{\tau_w}{\frac{1}{2}\rho u_e^2}$$

$$c_D = \frac{1}{\rho u_e^3} \int_0^{n_e} \tau \frac{\partial u}{\partial n} dn$$

$$H = \frac{\delta^*}{\theta}$$

$$\frac{d\theta^*}{ds} + 3 \frac{\theta^*}{u_e} \frac{du_e}{ds} = 2 c_D$$

$$\delta^* = \int_0^{n_e} \left(1 - \frac{u}{u_e}\right) dn, \quad \theta = \int_0^{n_e} \left(\frac{u}{u_e} - \frac{u^2}{u_e^2}\right) dn, \quad \theta^* = \int_0^{n_e} \left(\frac{u}{u_e} - \frac{u^3}{u_e^3}\right) dn$$

This is a set of 2 (OD) equations with 5 unknowns. (Though initially there are apparently 6, one other variable, which is typically either u_e or δ^* , depending on the approach to be used, is supplied.) To make progress, correlations (curve fits – i.e. additional equations – based on either numerical or experimental data) are introduced to provide the same number of equations as variables, thus closing the problem.

First, one more new variable (and correlation) is introduced in order to get the set into the forms required. This extra variable is $H^* = \theta^*/\theta$. After some more manipulation, the two ODEs above become

$$\frac{d\theta}{ds} + (2 + H) \frac{\theta}{u_e} \frac{du_e}{ds} = \frac{c_f}{2}$$

$$\theta \frac{dH^*}{ds} + H^*(1 - H) \frac{\theta}{u_e} \frac{du_e}{ds} = 2 c_D - H^* \frac{c_f}{2}$$

And correlations (different for laminar and turbulent flows) are introduced for

$$H^* = H^*(H, Re_\theta)$$

$$c_f = c_f(H, Re_\theta)$$

$$c_D = c_D(H, Re_\theta)$$

where $Re_\theta = \frac{u_e \theta}{\nu}$

Integral BL modelling: 2-equation methods — 2

For example, here are (laminar and turbulent) correlations relating dissipation coefficient, H , and Re_θ :

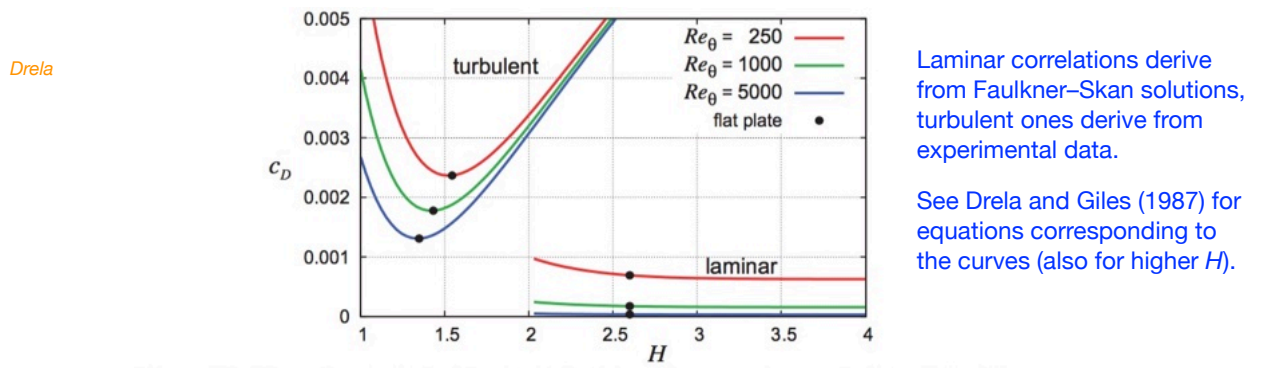


Figure 4.25: Dissipation coefficient for self-similar flows. Laminar values are listed in Table 4.1. Turbulent values are given by equation (4.100). Weak pressure gradients which displace H slightly from the flat plate value have little effect on c_D .

As noted above (and will see later), there are two typical cases one wishes to solve, ‘forward’ and ‘inverse’.

either **Forward** (given u_e , want δ^*).

or **Inverse** (given δ^* , want u_e).

$$\begin{aligned}\frac{d\theta}{ds} &= f_1(\theta, \delta^*, u_e) \\ \frac{d\delta^*}{ds} &= f_2(\theta, \delta^*, u_e)\end{aligned}$$

$$\begin{aligned}\frac{d\theta}{ds} &= f_3(\theta, \delta^*, u_e) \\ \frac{du_e}{ds} &= f_4(\theta, \delta^*, u_e)\end{aligned}$$

To proceed, the supplied pair of ODEs must be re-cast into one of these two forms.

Integral BL modelling: 2-equation methods — 3

In the forward (or direct) case, the two ODEs for θ and H^* are rearranged as a set of three equations

$$\begin{bmatrix} 1 & 0 & 2+H \\ -\frac{H}{H^*} \frac{dH^*}{dH} & \frac{H}{H^*} \frac{dH^*}{dH} & 1-H \\ 0 & 0 & 1 \end{bmatrix} \begin{pmatrix} \beta_\theta \\ \beta_{\delta^*} \\ \beta_{u_e} \end{pmatrix} = \begin{pmatrix} \frac{s}{\theta} \frac{c_f}{2} \\ \frac{s}{\theta} \left(\frac{2c_D}{H^*} - \frac{c_f}{2} \right) \\ \frac{s}{u_e} \frac{du_e}{ds} \end{pmatrix} \quad \text{where } \beta_\theta \equiv \frac{s}{\theta} \frac{d\theta}{ds}, \quad \beta_{\delta^*} \equiv \frac{s}{\delta^*} \frac{d\delta^*}{ds}, \quad \beta_{u_e} \equiv \frac{s}{u_e} \frac{du_e}{ds}$$

This we can solve with matrix inversion, numerical integration in s , and correlations already alluded to, in order to obtain θ and δ^* as functions of s , given $u_e(s)$.

In the inverse case, first defining $\beta_H = \beta_{\delta^*} - \beta_\theta$, we likewise solve

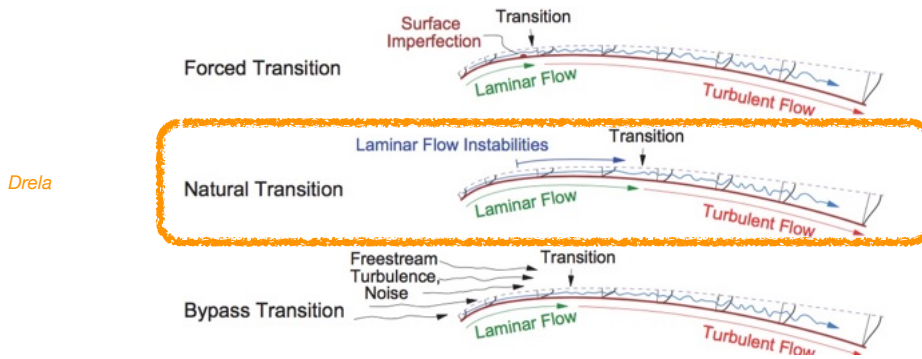
$$\begin{bmatrix} 1 & 0 & 2+H \\ 0 & \frac{H}{H^*} \frac{dH^*}{dH} & 1-H \\ 1 & 0 & 0 \end{bmatrix} \begin{pmatrix} \beta_\theta \\ \beta_H \\ \beta_{u_e} \end{pmatrix} = \begin{pmatrix} \frac{s}{\theta} \frac{c_f}{2} \\ \frac{s}{\theta} \left(\frac{2c_D}{H^*} - \frac{c_f}{2} \right) \\ \frac{s}{\delta^*} \frac{d\delta^*}{ds} \end{pmatrix}$$

in order to obtain θ and u_e as functions of s , given $\delta^*(s)$.

Both the above methods are able to integrate downstream through flow separations since the boundary layer shape factor H is calculated directly as part of the solution, and separation is accommodated by the correlations employed. One-equation methods fail when flow separation occurs, essentially because they have to assume H is a unique function of external pressure gradient (u_e), whereas in reality it is not.

A remaining issue is to predict where in s transition between laminar and turbulent BL occurs.

Transition prediction — 1



Prediction methods typically concentrate on modelling this case.

We start from a laminar state (at forward stagnation point) and attempt to predict the s -location at which 2D disturbances (Tollmien–Schlichting waves) will grow sufficiently in amplitude that they in turn become unstable to 3D disturbances and transition to turbulence ensues.

The basic methodology is to assume small flow disturbances (u, v) around an initially steady solution in the Navier–Stokes equations (the ‘base flow’ $U(n)$), which is taken as locally invariant in the s -direction.

It turns out that 2D (and 2-component) disturbances are the least stable in the case that the base flow is parallel (by Squire’s Theorem). The 2D incompressible disturbance equations, linearised for infinitesimal disturbances are

$$\begin{aligned} \frac{\partial u}{\partial t} + U \frac{\partial u}{\partial s} + v U' &= -\frac{\partial p}{\partial s} + Re^{-1} \nabla^2 u \\ \frac{\partial v}{\partial t} + U \frac{\partial v}{\partial s} &= -\frac{\partial p}{\partial n} + Re^{-1} \nabla^2 v \\ \frac{\partial u}{\partial s} + \frac{\partial v}{\partial n} &= 0 \end{aligned} \quad Re = \frac{U_e \delta}{\nu}, \quad U' \Rightarrow \frac{\partial U(n)}{\partial n}, \quad \text{etc.}$$

Transition prediction — 2

Taking the divergence of the momentum equations and exploiting incompressibility, $\nabla^2 p = -2U' \frac{\partial v}{\partial s}$ and using this with the n -momentum equation gives $\left[\left(\frac{\partial}{\partial t} + U \frac{\partial}{\partial s} \right) \nabla^2 - U'' \frac{\partial}{\partial s} - Re^{-1} \nabla^4 \right] v = 0$

Assuming wave-like disturbances $v = \hat{v}(n)e^{i(\alpha s - \omega t)}$, or equivalently $v = \hat{v}(n)e^{i\alpha(s - ct)}$ where $\omega = \alpha c$ gives

$$(U - c)(\hat{v}'' - \alpha^2 \hat{v}) - U'' \hat{v} + i(\alpha Re)^{-1}(\hat{v}'''' - 2\alpha^2 \hat{v}'' + \alpha^4 \hat{v}) = 0$$

$c = (\text{real}) \text{ wave speed}$
 $\alpha = (\text{complex}) \text{ wave number}$

which is the Orr–Sommerfeld equation, a 4th-order eigenvalue problem to be solved for the (eigen-)mode shape $\hat{v}(n)$ and eigenvalues $\Re(\alpha), \Im(\alpha), \omega \equiv \alpha_r, \alpha_i, \omega$ for supplied Reynolds number and base flow $Re, U(n)$.

Note that ω is real and that the disturbance grows in space (in the s -direction), with growth rate $-\alpha_i$.

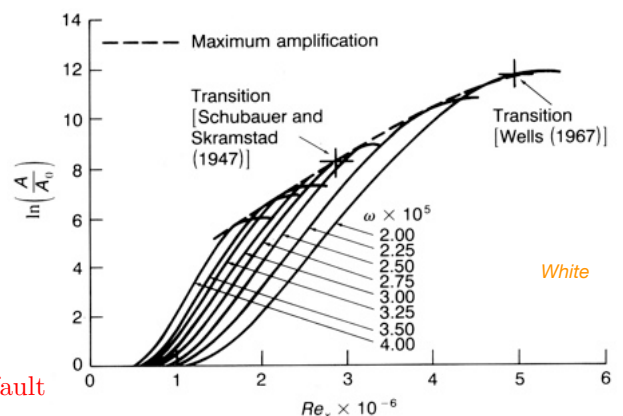
The total growth in disturbance amplitude is then given by

$$\frac{A}{A_0} = \exp \left[\int_{s_i}^{s_{tr}} (-\alpha_i) ds \right]$$

For a number of different values of ω , this amplitude ratio is found by solving the O–S eigensystem at each streamwise location, typically using Falkner–Skan BL shapes for local pressure gradient, then integrating the above. When A/A_0 reaches some ‘large’ value $e^{N_{crit}}$, transition is deemed to occur.

Typical values

$N_{crit} = 4$;	noisy wind tunnel
$N_{crit} = 9$;	quiet wind tunnel, XFOIL default
$N_{crit} = 11$;	sailplane in flight



Transition prediction — 3

To use this method, one needs to have available or be able to compute the growth rate $-\alpha_i$ as a function of position in s (BL thickness) and oscillation frequency ω . Shown below are examples of such data from Jaffe, Okamura and Smith, *AIAA J* **8**(2): 301–308, (1970).

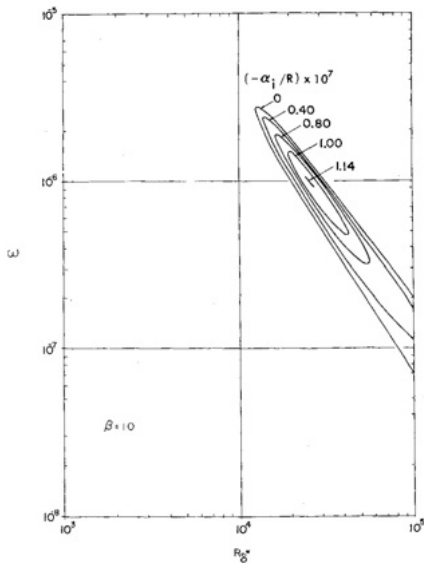


Fig. 1 Stability chart—stagnation point flow.

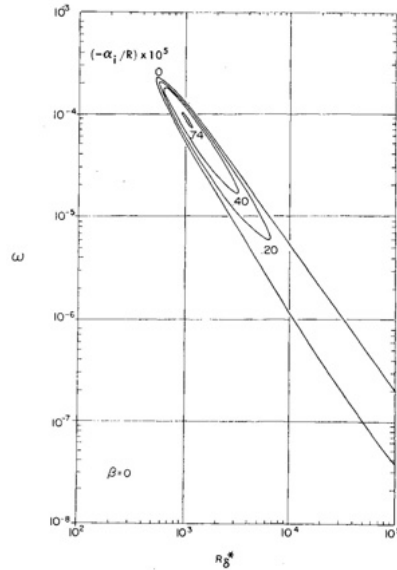


Fig. 2 Stability chart—flat plate flow.

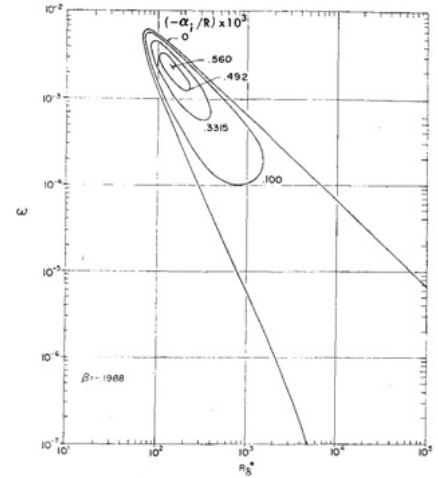


Fig. 3 Stability chart—separating flow.

Jaffe et al.

XFOIL precomputes a look-up table of growth rates for Falkner–Skan profiles to obtain local growth rates.

Viscous-inviscid interaction (VII)

VII

The basis of the approach is to solve separately the inviscid and viscous portions of the flowfield and then to match the two solutions to obtain a valid solution everywhere.

Topics

1. Boundary conditions and the choice of matching surface.
2. BL separation and the failure of classical matching.
3. Alternative matching strategies: inverse and semi-inverse.

Recap

1. Inviscid flow: panel method (Laplace's equation)
 - a. Prescribed stream function BC: $\psi = \psi_0$.
 - b. No flow-through BC: $\mathbf{u} \cdot \mathbf{n} = \partial\Phi/\partial n = 0$.
2. Viscous flow: integral BL analysis e.g.:

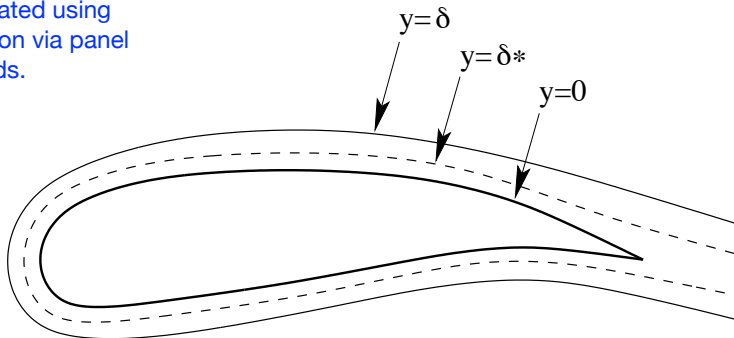
$$\frac{d\theta}{dx} + (2 + H) \frac{\theta}{U_e} \frac{dU_e}{dx} = \frac{C_f}{2}; \quad \begin{cases} H = H(\theta, U_e) \\ C_f = C_f(\theta, U_e) \end{cases}$$

We note that this ODE can be solved either for θ or U_e .

- a. Direct method: given U_e , get θ .
- b. Inverse method: given θ , get U_e .

Position of the matching surface

Far-field flow is effectively inviscid, calculated using Laplace's equation via panel methods.



BL flow solved typically via integral method, displaces fluid away from surface.

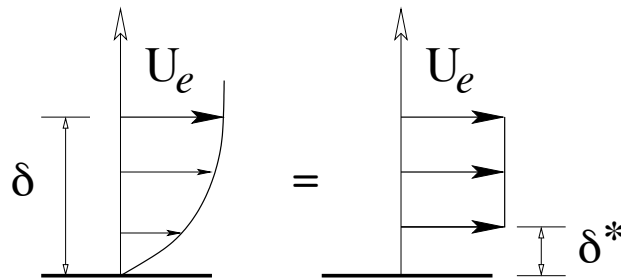
Goal: match the two solutions in a consistent method that allows both far-field and BL flows to be correct.

Alternative matching strategies/locations:

1. Displacement surface: $y = \delta^*$.
2. Entrainment velocity at edge of BL: $y = \delta$.
3. Transpiration velocity: blowing at $y = 0$.

Match at $y=\delta^*$: displacement surface

The idea is to increase the body thickness by δ^* .



Procedure:

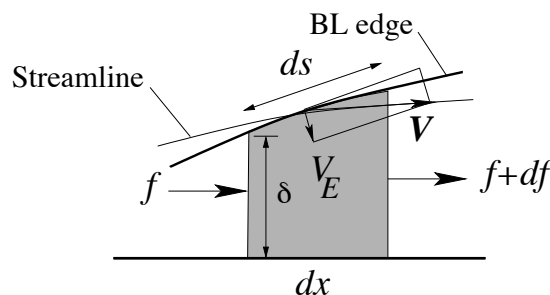
1. For a given airfoil shape $y(x)$ calculate inviscid solution U_e ;
2. Given U_e , calculate viscous BL solution $\Rightarrow \delta^*$;
3. Displace the airfoil surface to get new airfoil shape $y_n(x)=y(x) + \delta^*$;
4. If $\delta^*=0$ stop, else $y(x)=y_n(x)$ and repeat.

Problems:

1. The panelling and influence coefficients have to be remade at each iteration.
2. Method fails when separation is present.

Match at $y=\delta$: entrainment velocity

Let us denote the velocity normal to the edge of the BL by V_E and $f = \int_0^\delta u \, dy$



By continuity, $V_E \, ds = df$, and assuming $ds \approx dx$ we have

$$V_E = \frac{d}{dx} \int_0^\delta u \, dy$$

$$= \frac{d}{dx} \left[U_e \int_0^\delta \left\{ 1 - \left(1 - \frac{u}{U_e} \right) \right\} dx \right]$$

A BL solution gives us δ and δ^* . As boundary condition for the inviscid solver we prescribe, at $y=\delta$, the normal velocity

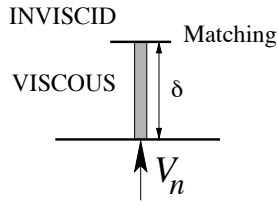
$$V_E = \frac{d}{dx} [U_e(\delta - \delta^*)]$$

Again: the panelling and influence coefficients have to be recomputed at each iteration.

Match at $y=0$: transpiration velocity

The idea is to derive a transpiration velocity at the airfoil surface that displaces fluid by a correct amount, then use this result as a BC for inviscid flow analysis.

Advantage: airfoil shape remains invariant.



$$\begin{aligned} \frac{\partial u_i}{\partial x} + \frac{\partial v_i}{\partial y} &= 0; \quad \text{Inviscid} \\ \frac{\partial u}{\partial x} + \frac{\partial v}{\partial y} &= 0; \quad \text{Viscous} \end{aligned} \quad \text{Then} \quad \frac{\partial}{\partial x}(u_i - u) + \frac{\partial}{\partial y}(v_i - v) = 0$$

Integrate across BL $\int_0^\delta \frac{\partial}{\partial x}(u_i - u) dy + [v_i - v]_0^\delta = 0$

Impose appropriate BCs to obtain the value of the transpiration velocity V_n as follows

- $y = 0 : v = 0, v_i = V_n$
- $y = \delta : v = v_i$ (matching condition)

This gives:
$$V_n = \int_0^\delta \frac{\partial}{\partial x}(u_i - u) dy$$

Assuming $\partial\delta/\partial x \approx 0$
$$V_n \approx \frac{d}{dx} \int_0^\delta (u_i - u) dy$$

Finally, using $u_i = U_e$ we get
$$V_n \approx \frac{d}{dx} \int_0^\delta U_e \left(1 - \frac{u}{U_e}\right) dy \Rightarrow V_n \approx \frac{d}{dx} [U_e(x) \delta^*(x)]$$

To obtain an 'equivalent inviscid flow' we must prescribe V_n as a BC to the inviscid solver.

Failure of classical matching with flow separation

Prescribing U_e is equivalent to prescribing the pressure gradient, which is incorrect in the presence of interaction since:

1. This leads to Goldstein's singularity, i.e. solutions that behave as

$$\tau_w \propto \frac{\partial u}{\partial y} \sim (x_s - x)^{1/2}$$

where x_s is the position of the separation point. Using continuity, it is found that v becomes infinite at $x=x_s$ (breaking the BL assumptions).

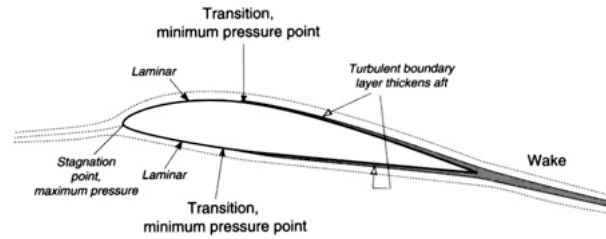
2. Significant curvature of the boundary layer streamlines forces an adjustment of pressure in the streamline direction, and, at separation, in the normal direction.

In practice, VII overcomes these problems once the BL and inviscid flow solutions are fully coupled, as the singularity is removed once U_e is computed as part of the solution (Catherall & Mangler JFM **26**, 1966).

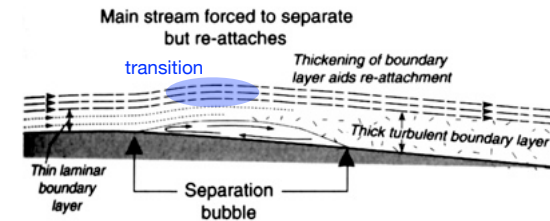
We will take a closer look at the the observed physics of flow separation and in particular separation bubbles.

Boundary layer separation bubbles – 1

1. Boundary layer separation does not always occur — there may be a direct transition to turbulence and typically the resulting BL can stay attached up to stall.



2. Typically, if the separating BL is laminar, the separated shear layer undergoes transition and will likely reattach. Recirculating laminar flow within bubble is slow.



3. Details of the separation bubble, and whether the resulting turbulent BL may subsequently separate (i.e. incipient TE stall) depends on Re and α , and of course the airfoil shape.

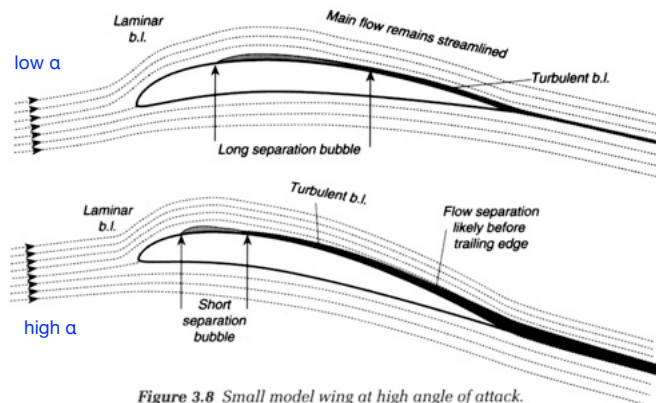
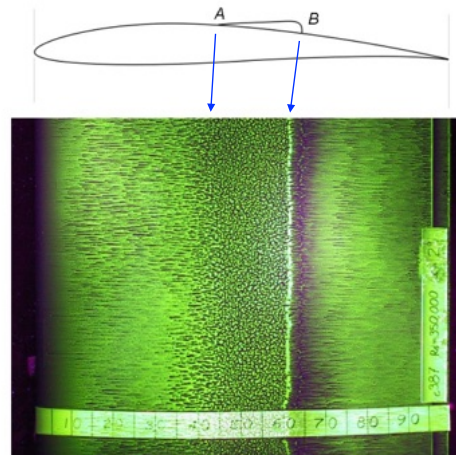


Figure 3.8 Small model wing at high angle of attack.

Length of the separation bubble scales roughly with Re : at quite low Re , reattachment may not occur.

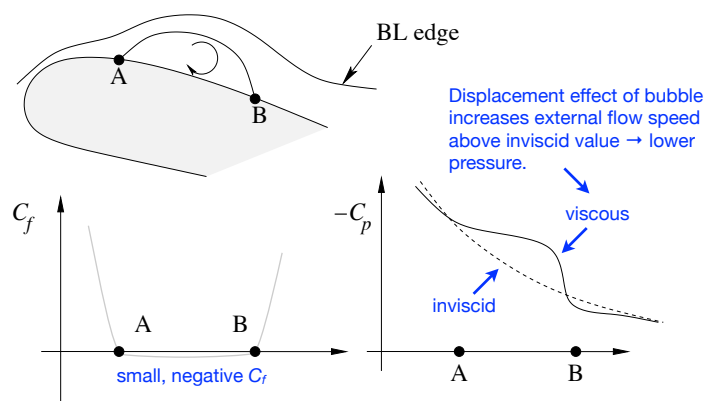
Boundary layer separation bubbles – 2

4. Flow separation and separation bubbles can be detected using flow visualisation, typically using dye in a light mineral oil.



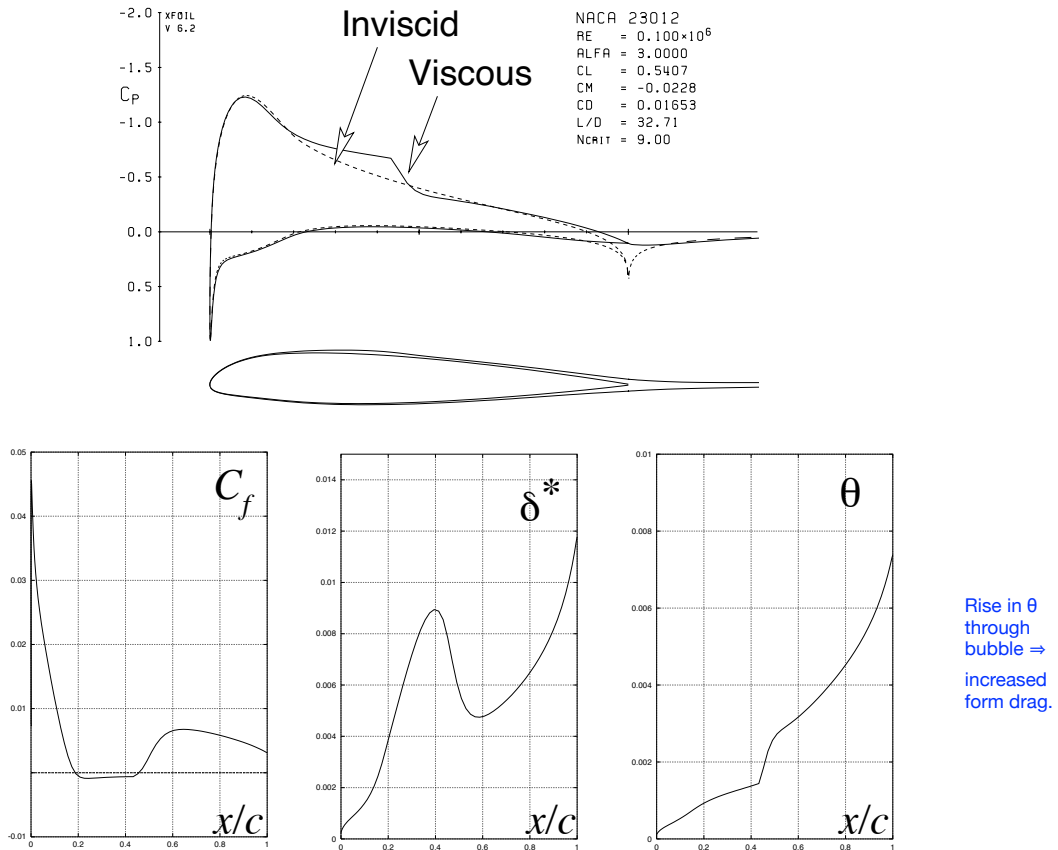
Here is the top view of an airfoil treated in this way in a wind tunnel test ($Re=3.5 \times 10^5$, $\alpha=2^\circ$). Attached BL flow is laminar upstream of separation line, turbulent downstream of reattachment line.

5. The signature of a separation bubble is readily recognised in measurements or computations of surface pressure and skin friction.



Boundary layer separation bubbles – 3

6. Effect of airfoil separation bubble on BL parameters.

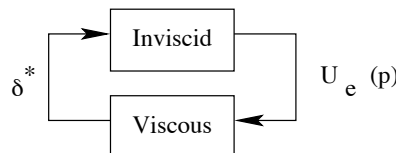


VII solution strategies

e.g. Lock & Williams (*Prog Aerosp Sci* 1987)

Classical: δ^* is (or helps provide) BC for inviscid solver and U_e is BC for viscous BL solver.

See preceeding notes on integral BL modelling for forward and inverse means of treating the BL equations.

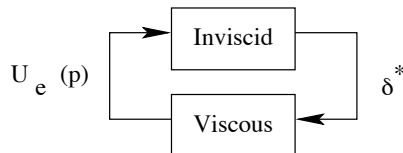


Given δ^* determine U_e .

Given U_e determine δ^* (\Rightarrow transpiration).

Example coupling between solutions: $V_n = \frac{d}{dx} [U_e(x)\delta^*(x)]$

Inverse: U_e is BC for inviscid solver and δ^* is BC for viscous BL solver. Both of these are solved in inverse mode.



Given U_e determine transpiration ($\Rightarrow \delta^*$).

Given δ^* determine U_e .

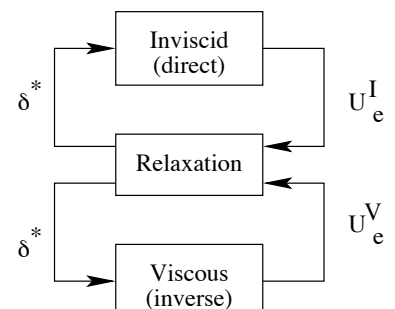
Semi-inverse: Combine the two above approaches, with relaxation.

1. Use δ^* to calculate U_e^I (direct) and U_e^V (inverse).

2. Use a velocity correction to obtain the new δ^*

$$\delta_{i+1}^* = \delta_i^* \left\{ 1 + \beta \left(\frac{U_e^V}{U_e^I} - 1 \right) \right\}$$

where $\beta \approx 0.2$ is a relaxation parameter.



XFOIL VII code

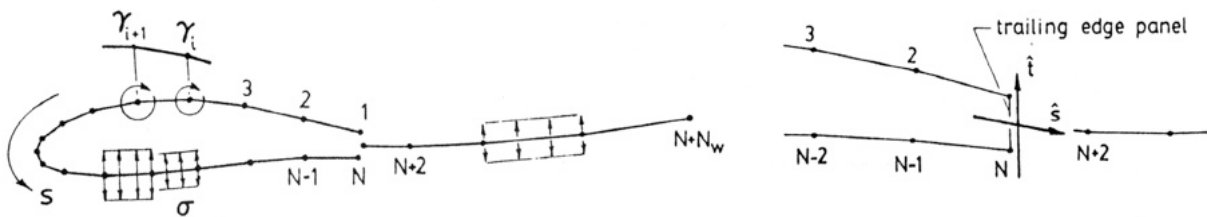


<http://web.mit.edu/drela/Public/web/xfoil/>

See also <http://cobweb.ecn.purdue.edu/~aae333/XFOIL/Tutorial/Tutorial%20for%20XFOil.htm>

Background & capabilities

XFOIL uses a combination of linear vorticity strength distribution with constant source strength on each panel and in the wake (to provide transpiration velocities).



Capabilities:

1. Viscous (or inviscid) analysis of an existing airfoil, allowing
 - forced or free transition
 - transitional separation bubble(s)
 - limited trailing edge separation
 - lift and drag predictions just beyond C_{Lmax}
 - Karman-Tsien compressibility correction
2. Airfoil design and redesign by interactive specification of a surface speed distribution in two methods:
 - Full-Inverse, based on a complex-mapping formulation
 - Mixed-Inverse, an extension of XFOIL's basic panel method
3. Airfoil redesign by interactive specification of new geometric parameters such as
 - new max thickness and/or camber
 - new LE radius
 - new TE thickness
 - new camber line via geometry specification
 - new camber line via loading change specification
 - flap deflection
 - explicit contour geometry (via screen cursor)
4. Blending of airfoils.
5. Drag polar calculation with fixed or varying Reynolds and/or Mach numbers.
6. Writing and reading of airfoil geometry and polar save files.
7. Plotting of geometry, pressure distributions, and polars.

Usage & examples – 1

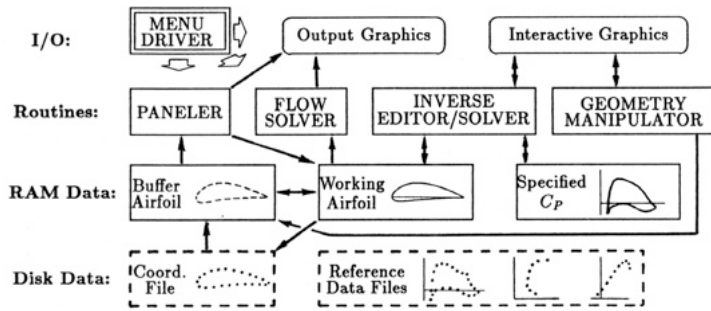
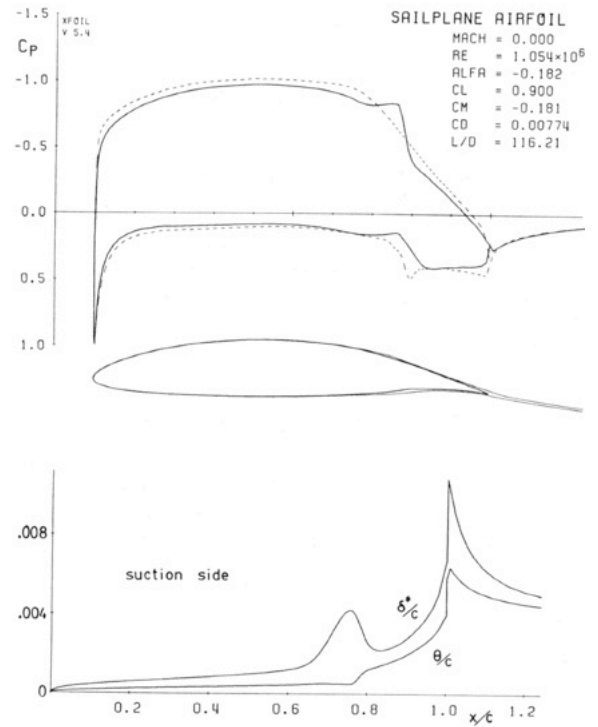
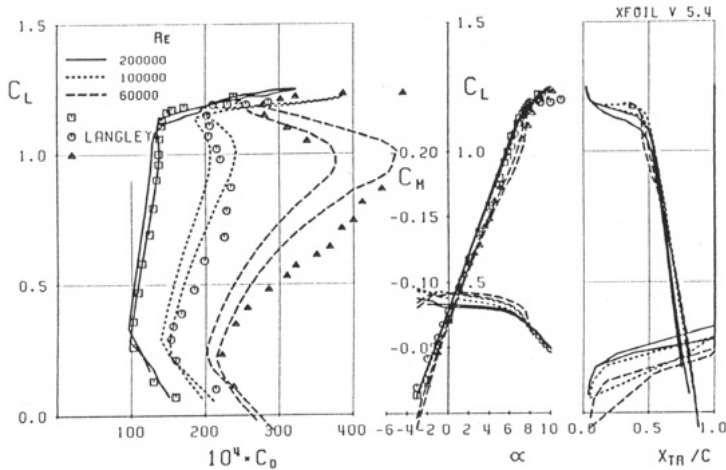
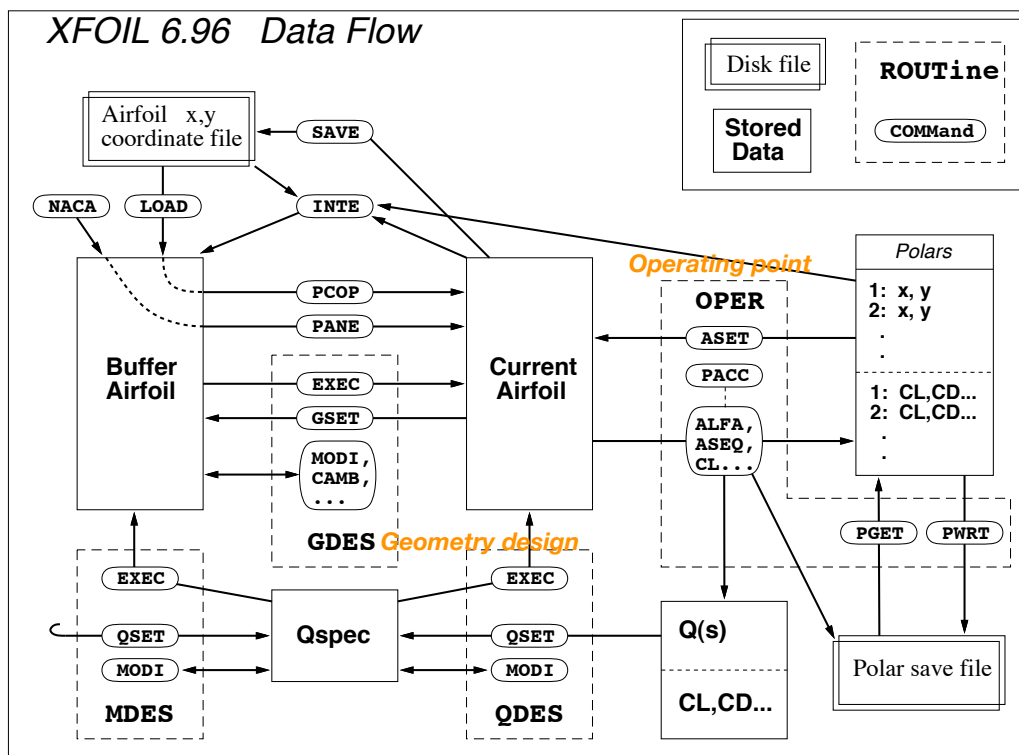


Fig. 13 XFOIL airfoil design/analysis system.



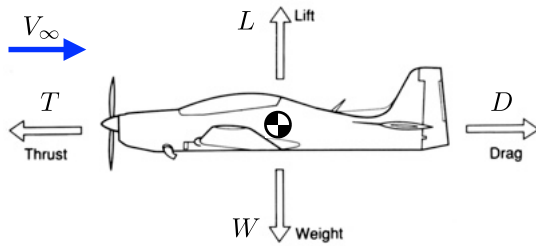
Usage & examples – 2



Design via complex mapping

Design via speed specification

Usage & examples – 3 ('Type 2' polar analysis)



Lift = weight in trimmed level flight

$$\frac{1}{2}\rho V^2 SC_L = L = nW = W$$

Mean wing chord \bar{c}

Wing area $S = b\bar{c}$

Aspect ratio $A = \frac{b^2}{S} = \frac{b}{\bar{c}}$

Mean chord Reynolds number $Re = \frac{\rho V \bar{c}}{\mu} = \frac{V \bar{c}}{\nu}$

Rearrange $\frac{1}{2}\rho V^2 SC_L = W$ to obtain $V\sqrt{C_L} = \sqrt{\frac{2W}{\rho S}}$

$$Re\sqrt{C_L} = \frac{\rho \bar{c}}{\mu} \sqrt{\frac{2W}{\rho S}} = \frac{1}{\mu} \bar{c} \sqrt{\frac{2\rho W}{S}} = \frac{1}{\mu} \sqrt{2\rho \frac{\bar{c}^2}{S} W} = \frac{1}{\mu} \sqrt{\frac{2\rho W}{A}} \equiv \frac{1}{\nu} \sqrt{\frac{2W}{\rho A}}$$

For an aircraft at fixed W , $Re\sqrt{C_L}$ is a (dimensionless) constant in trimmed level flight.

This the quantity held fixed in an XFOIL Type 2 polar analysis: as C_l increases, Re decreases.

(Holding only Re alone fixed – a Type 1 analysis – is not directly relevant to varying C_l in level flight)

Key features of interpretation for XFOIL results

1. $C_f < 0$ implies flow reversal: either separation bubble or just separation
2. Often a separation bubble is accompanied by a plateau in C_p
3. Xfoil reports predicted transition locations - use this in interpretation
4. Examine $H = \delta^*/\theta$, consider values typical of laminar/turbulent/reversed flow
5. Interpretation of BL features (e.g. dissipation and its integral) w.r.t. drag production
6. When and how to use a Type 2 analysis

NB: Though we described solving VII using forward, inverse and mixed methods, in fact XFOIL solves the entire VII problem iteratively using a coupled Newton–Raphson type method. It is typically helpful to increase the maximum number of iterations taken above the XFOIL default value of 20 (to something more like 100), especially for sequenced solves required in drag polar accumulation.

Sometimes, as is typical of N–R methods, the iteration fails to converge even with a large number of iterations. Try clearing the BL variables and restarting, or try restarting from a lower C_l .

NB: in ANY analysis involving a meshed/discrete approximation of a continuous problem, you should CHECK the effect of mesh refinement on your calculated outcomes.

Airfoil design for C_{lmax}

Background

Airfoil design for C_{lmax} contains a few topical areas, linked by the fact that maximum lift is limited by flow separation/stall.

1. In order to fly slowly/avoid stalling, we just want C_l to be as high as possible, with low drag generally a secondary consideration — sometimes, high drag may not be so bad. This is often achieved with variable section geometry/multi-element airfoils, or other high-lift devices — the aircraft's 'high-lift system'.
 - a. Conventional airfoils: $C_{lmax} \approx 1.3-1.7$, depending on Re , t/c , surface roughness, camber.
 - b. For a single-element airfoil the maximum achievable is $C_{lmax} < 3.05$.

$$V_{stall} = \sqrt{\frac{2}{\rho} \frac{W}{S} \frac{1}{(C_L)_{max}}}$$

2. When manoeuvring, rate of turn ω is maximum when flying at the 'corner speed', determined by C_{lmax} in a clean configuration. Sometimes this is pushed above the undeformed airfoil's value by using manoeuvre flaps/slats.

$$V_c = \sqrt{\frac{2}{\rho} \frac{W}{S} \frac{(n)_{limit}}{(C_L)_{max}}}$$

3. For minimum sink speed V_s when gliding, or to maximize duration in (propeller)-powered flight, we want the airfoil 'power factor' ($C_l^{3/2}/C_d$) to be as large as possible. Typically

$$V_s \approx \sqrt{\frac{\rho}{2} \frac{W}{S} \frac{C_d^2}{C_l^3}}$$

(Plain) airfoil $C_{l_{max}}$

1. The high-lift problem is to develop maximum lift in the presence of a BL, i.e. how to avoid separation.
2. This can be achieved if required through geometry changes or in extreme cases (e.g. when wing loading is very high) with augmentation by airfoil BL suction or blowing.
3. The methods for predicting $C_{l_{max}}$ are a blend of theory and empirical relations since $C_{l_{max}}$ is determined by flow separation which is very difficult to reliably compute for curved surfaces.
4. CFD does not provide reliable answers as yet.
5. Correlations exist for some families of airfoils. E.g. at $Re=8 \times 10^6$, $C_{l_{max}}$ for NACA 4-digit airfoils can be estimated from

$$C_{l_{max}} \approx 1.67 + 7.8pz - 2.6 \frac{(0.123 + 0.22p - 0.5z - t)^2}{t^{3/2}}$$

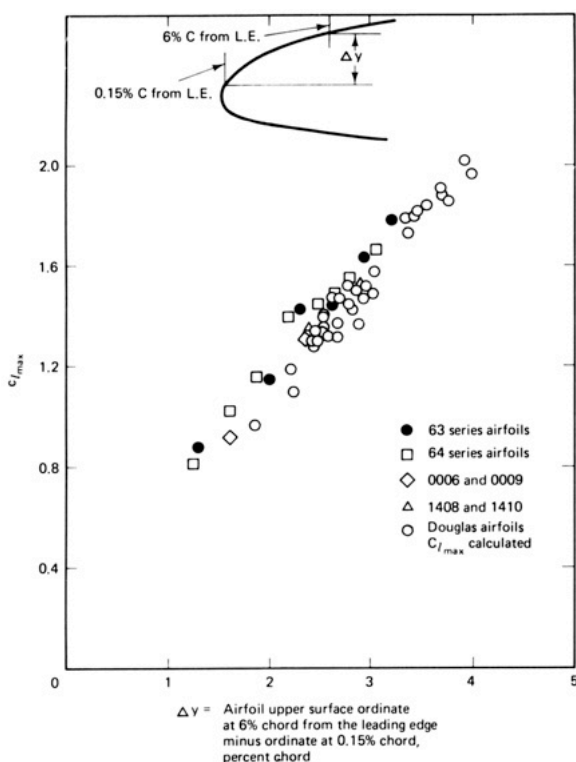
where p , t and z are respectively the dimensionless (i.e. normalized by c) values for position of maximum camber, maximum thickness, and maximum camber.

6. More general/extensive methods based largely on correlations of experimental results are published e.g. by ESDU.
7. We will first examine the gross effects of thickness, LE radius etc on $C_{l_{max}}$.

Influence of geometric features on $C_{l_{max}}$

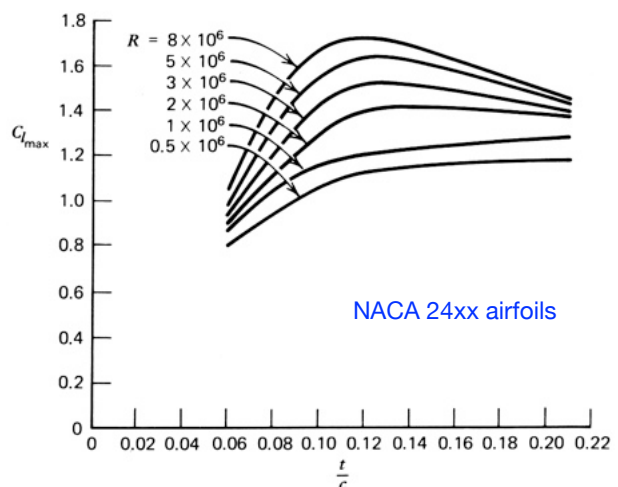
1. Nose radius/LE shape.

Larger radius tends to reduce adverse pressure gradient peak value.



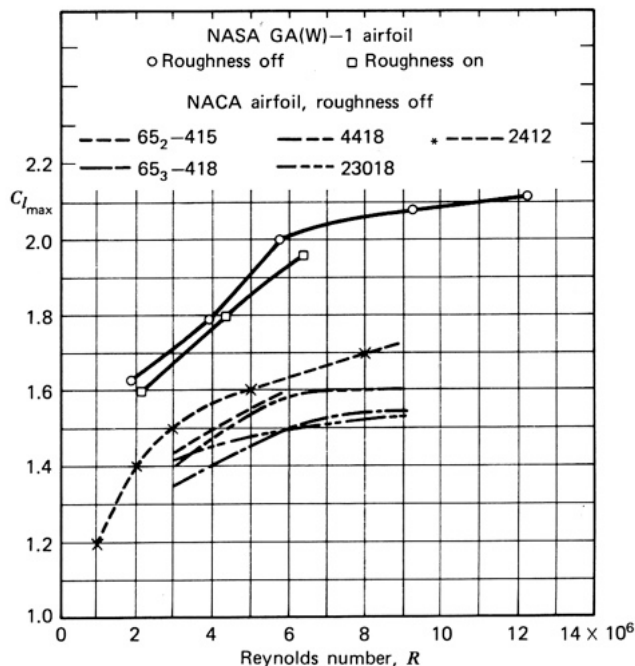
2. t/c ratio (and Re).

Increasing thickness increases peak suction but also makes recovery pressure gradient increasingly adverse — there is a 'happy medium'.



Influence of Re and surface roughness on $C_{l,max}$

1. Increasing Re makes BL δ/c lower and generally reduces risk of separation.
2. Roughening the airfoil surface increases skin friction, increases δ/c , increases risk of separation*.



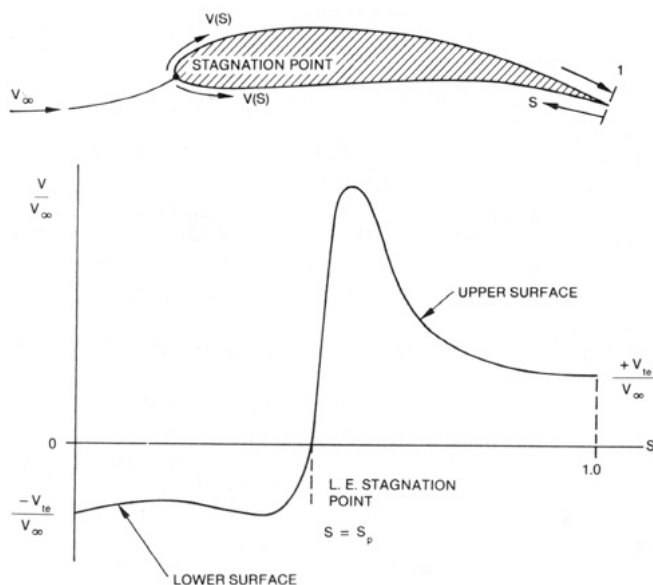
Caveat: these statements presume Re is high enough that BL transition occurs.

* Paradoxically, at low Re , increasing roughness may promote transition and then *enhance* BL resistance to separation in an adverse PG, thereby increasing $C_{l,max}$. This is called BL turbulation.

Airfoil design for high lift — 1

While values of $C_{l,max}$ for individual airfoils are largely obtained experimentally, methods have been developed for *design* of airfoils for $C_{l,max}$, based on quasi-empirical separation criteria.

The idea is to achieve a maximum C_l without BL separation and also a realistic airfoil shape.



Typical velocity distribution around an airfoil.

Note that one is not completely free to specify this distribution arbitrarily, as the velocities must match at the LE and TE (Kutta condition), **and** the farfield velocity must approach a uniform value (ellipticity of potential flow connects this back to the values on the airfoil). In practice the methods are semi-iterative and can cope with these requirements, regardless of ICs.

To obtain high lift, we want

- (a) the upper surface pressure to be as low as possible, and
- (b) the lower surface pressure as high as possible, i.e. as close to stagnation as possible.

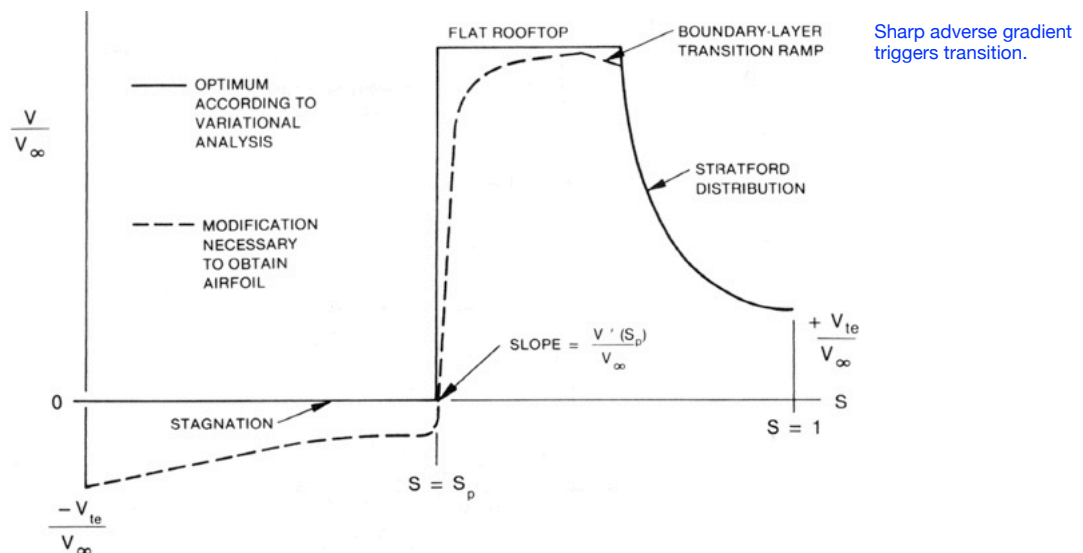
Most of the difficulty comes in achieving the first of these without flow separation.

Airfoil design for high lift – 2

Objectives

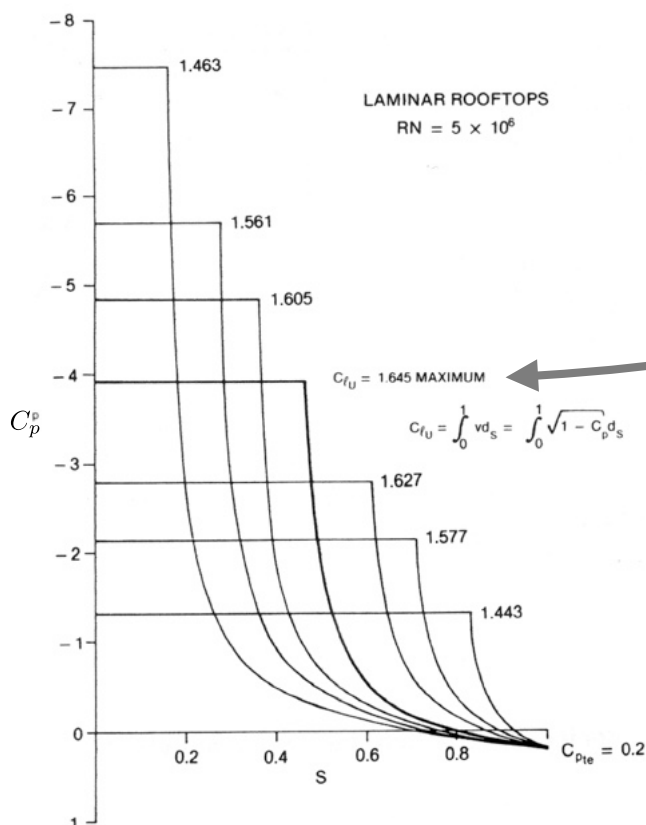
1. Achieve the highest integrated C_p differential between pressure and suction surfaces.
2. Retain laminar flow as close as practicable to the TE to reduce drag.
3. 'Trip' BL to make it turbulent and so more able to sustain an adverse pressure gradient.
4. Avoid separation of resulting turbulent BL.

The optimal distribution is obtained using a semi-empirical relationship that predicts turbulent BL separation in an adverse PG. The turbulent BL is then always about to separate from the upper pressure recovery surface. (Stratford, 1959. Liebeck 1970s).



Airfoil design for high lift – 3

Family of optimised upper-surface pressure distributions designed according to Stratford's criterion.

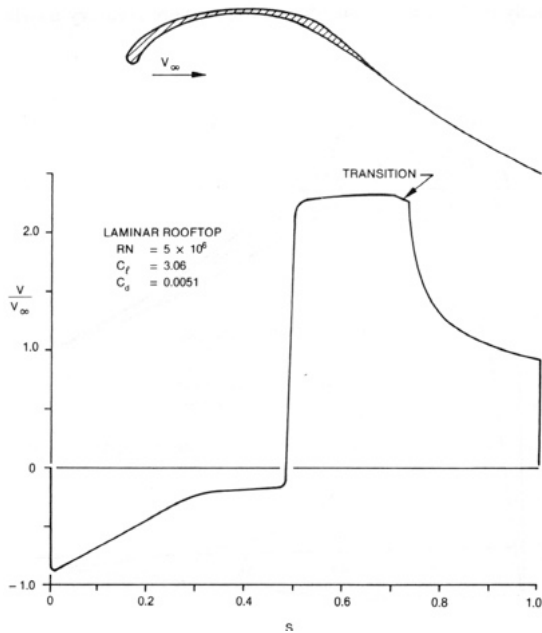


Of a set of recovery curves that satisfy Stratford's imminent separation criterion, the one that provides the greatest area is optimal.

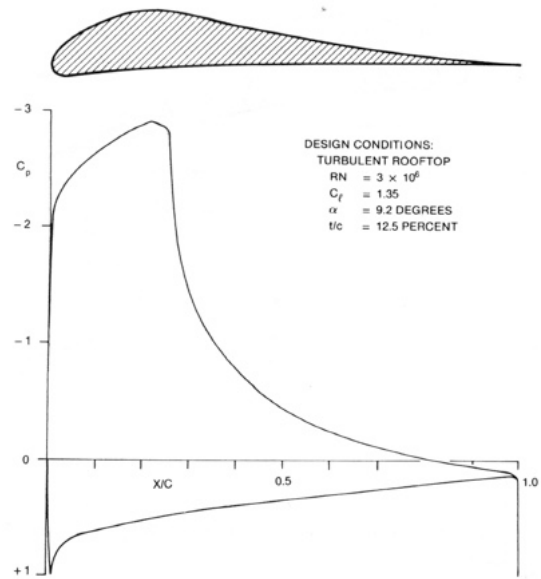
Case study – Liebeck airfoils

Examples

Liebeck's maximum lift airfoil.



A more realistic compromise.



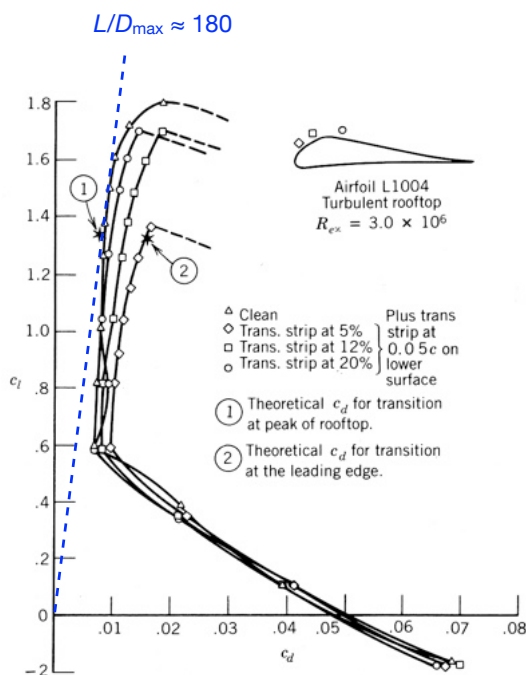
McCormick

Case study – Liebeck airfoils

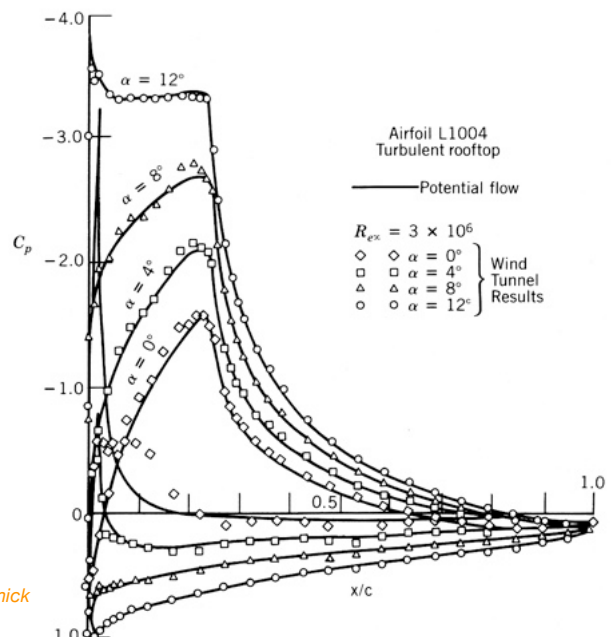
Performance

As well as high C_{lmax} , C_l/C_{dmax} , $C_l^{3/2}/C_{dmax}$ are very good too.

Experimental vs. computed results.



McCormick



However! L/D performance at low C_l (i.e. high speed) is poor — and these airfoils have not been widely applied.

Airfoil design to influence separation bubbles

Design to influence separation bubble behaviour

Separation bubbles are very common and at moderate to low Reynolds numbers, may contribute substantially to profile drag. Skin friction is typically very low within such bubbles.

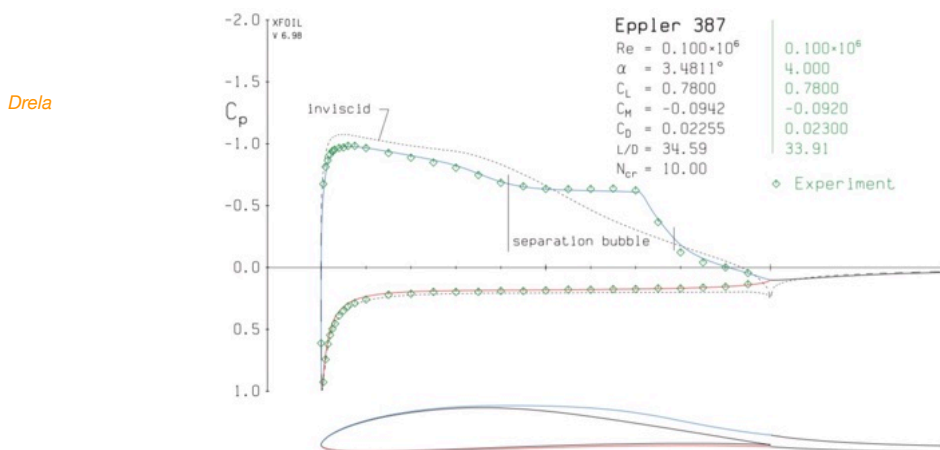


Figure 4.34: XFOIL [5] pressure distributions on Eppler 387 airfoil at $Re = 100\,000$ reveal a transitional separation bubble on the upper surface. Experimental data is from McGhee et al [42].

Drag per unit width: $D' = P_\infty = \int_{\text{airfoil}} \tau_w ds + \int_{\text{airfoil}+\text{wake}} -\rho u_e \delta^* \frac{du_e}{ds} ds$ where P is momentum defect.

$$\frac{dP}{ds} = \tau_w - \delta^* \frac{dp}{ds} \quad \text{or equivalently} \quad \frac{d}{ds}(\rho u_e^2 \theta) = \tau_w - \rho u_e \delta^* \frac{du_e}{ds} \quad \text{or, again} \quad \frac{1}{\rho u_e^2 \theta} \frac{d}{ds}(\rho u_e^2 \theta) = \frac{c_f}{2\theta} - \frac{H}{u_e} \frac{du_e}{ds}$$

Design to influence separation bubble behaviour

Now in a separation bubble, skin friction is small, so $\frac{1}{\rho u_e^2 \theta} \frac{d}{ds} (\rho u_e^2 \theta) \approx -\frac{H}{u_e} \frac{du_e}{ds}$

Or, considering losses through separation bubble $\frac{\Delta \rho u_e^2 \theta}{(\rho u_e^2 \theta)_{\text{avg}}} \approx -H_{\text{avg}} \frac{\Delta u_e}{(u_e)_{\text{avg}}}$

So, the larger the change in u_e and the larger the average value of H through the bubble, the larger the total momentum defect and 'bubble drag' contribution to total drag.

The ideal is to arrange transition to occur as close as possible downstream of onset of separation.

This may be achieved by careful airfoil shape tuning with minimal upstream increase in H (to promote instability and transition early in the bubble).

This is known as 'transition ramp' tailoring.

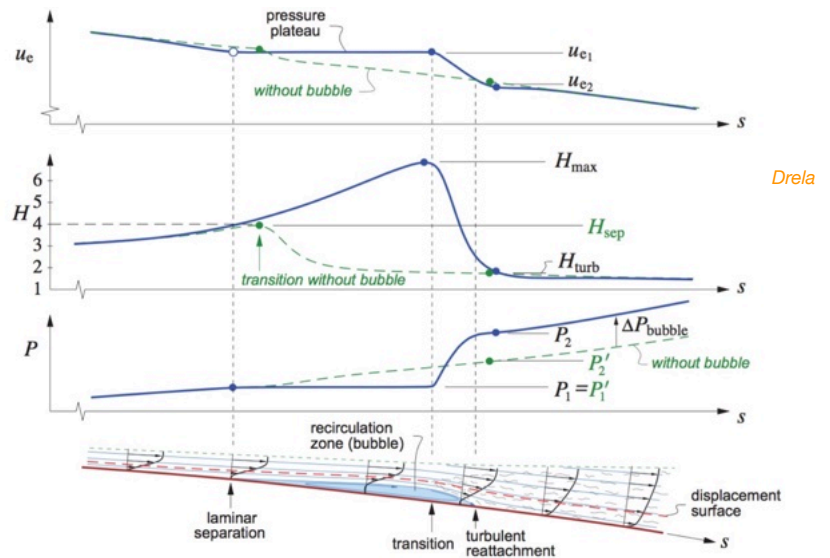


Figure 4.35: Transitional separation bubble is produced when laminar separation is followed by transition and subsequent reattachment. The excess momentum defect increase ΔP_{bubble} due to a large H_{max} is a bubble drag penalty.

Case study 1: E387 vs SD7037

$Re = 100,000$; $C_l = 0.78$.

Drela

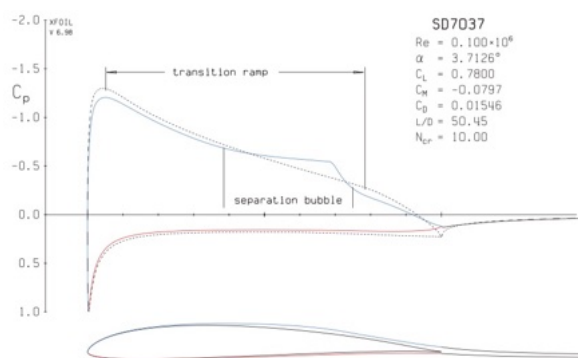


Figure 4.36: XFOIL [5] pressure distributions on SD7037 airfoil at $Re = 100,000$, which features a long transition ramp (weak adverse pressure gradient) starting at $x/c \approx 0.05$ to reduce bubble loss.

For the same Re and C_l , fairly subtle shape changes to intentionally affect separation bubble behaviour have increased L/D from 35 for the E387 to over 50 for the SD7037.

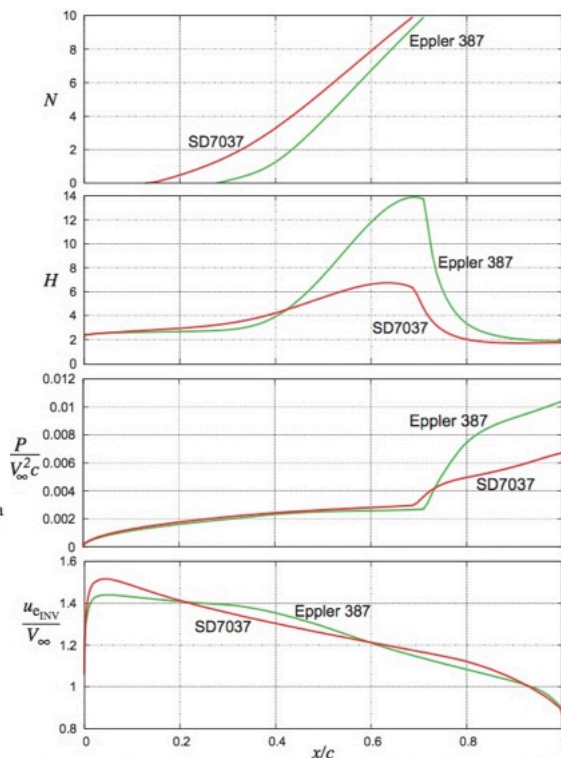
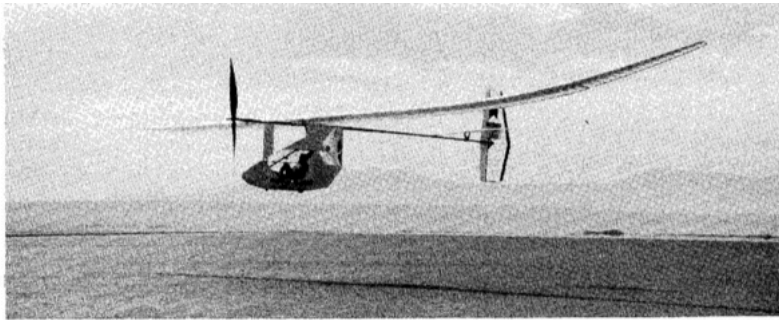


Figure 4.37: Upper surface inviscid edge velocity distributions and resulting shape parameter and TS-wave envelope distributions for SD7037 and Eppler387 airfoils. Long and shallow transition ramp in the $u_e(x)$ distribution of the SD7037 airfoil produces a smaller maximum H value and a smaller u_e decrease over the bubble. The result is a much smaller rise in the momentum defect P past transition at $x/c \approx 0.7$ for the SD7037 compared to the Eppler387. The SD7037 has 32% less drag as a consequence.

Case study 2: human-powered aircraft

Daedalus flew 115 km from Crete to Santorini in 1988, taking just under 4 hours (ferry takes 3 hours).

Re approx 0.5M.



A great deal of effort was put into airfoil design and into affecting separation bubble behaviour (see Drela *J Aircraft* **25**: 724, 1988.)

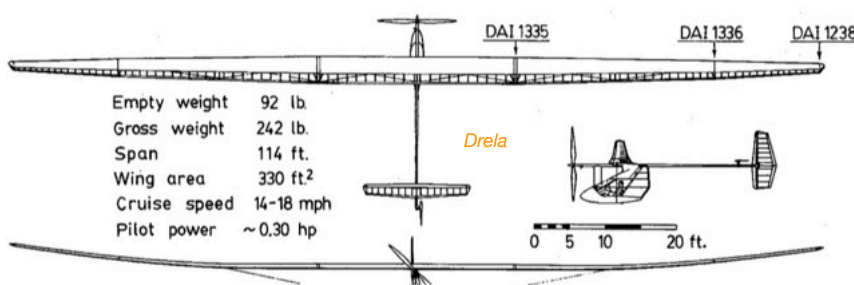


Fig. 1 The Light Eagle human-powered aircraft.

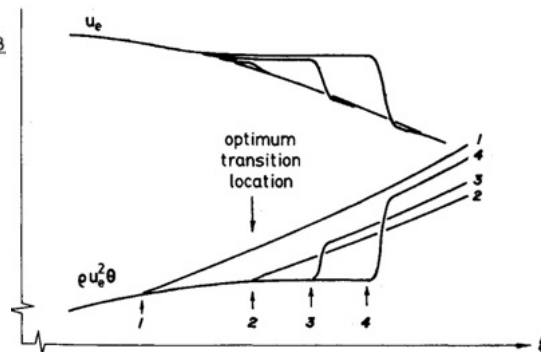


Fig. 3 Effect of transition location on bubble size and loss.

Case study 2: human-powered aircraft

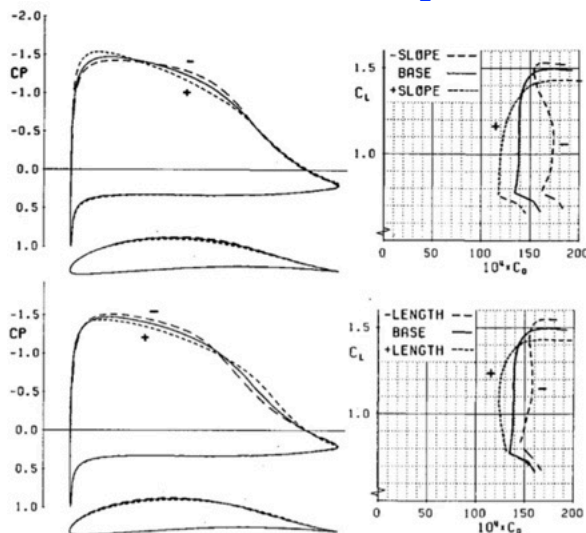


Fig. 6 Effect of transition ramp slope and length on performance: design $C_L = 1.2$, $Re = 250,000$.

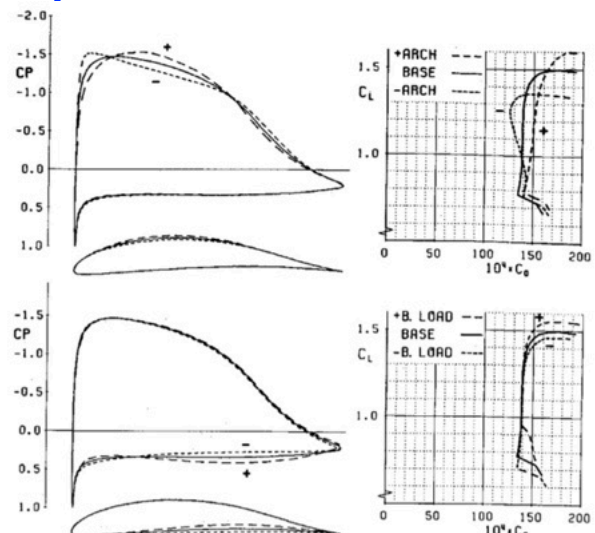


Fig. 7 Effect of transition ramp arch (design $C_L = 1.2$) and bottom loading (upper $C_p \approx \text{const}$) on performance: $Re = 250,000$.

Table 1 Effects of aerodynamic design parameters

Increasing	Increases	Decreases
Ramp length	C_M	Bubble loss, friction drag, C_{Lmax}
Ramp slope	Poor surface degradation	C_M , bubble loss, C_{Lmax}
Ramp arch	Bubble loss, C_{Lmax} , α range	Poor surface degradation
Bottom loading	C_M , C_{Lmax}	Thickness, α range
Recovery concavity	C_{Lmax} , bubble loss	Aft thickness, drag creep

These kinds of changes can be examined using 'mixed inverse' capabilities of XFOIL.

Case study 3: pitfalls of (machine-based) airfoil optimisation

Drela in *Frontiers of Computational Fluid Dynamics*, AIAA 1998.

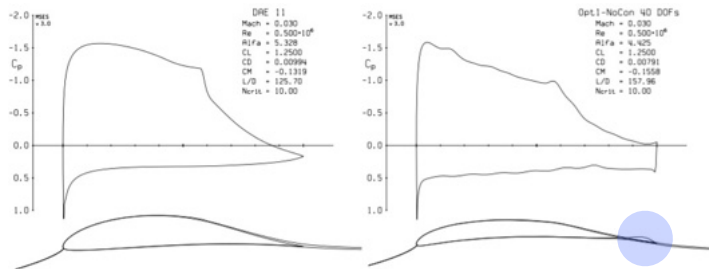


Figure 1: Baseline DAE-11 airfoil, and partially-optimized unconstrained airfoil.

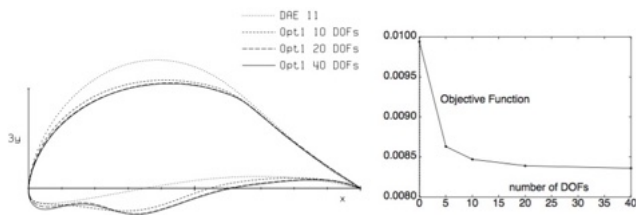


Figure 2: One-point optimized airfoil geometry and objective function versus number of design DOFs.

Optimised. But off-design performance is worsened.

Optimised. But impractical (re-entrant shape).

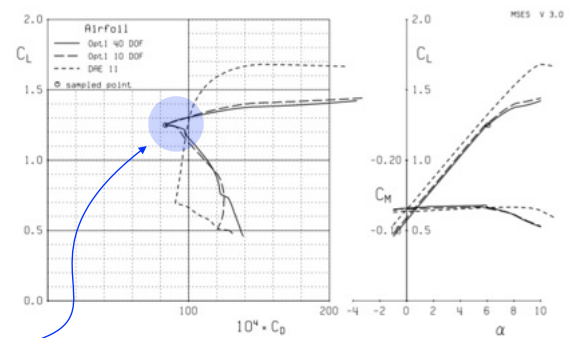


Figure 3: Polars for original DAE-11 airfoil and 1-point optimized airfoils.

Case study 3: pitfalls of (machine-based) airfoil optimisation

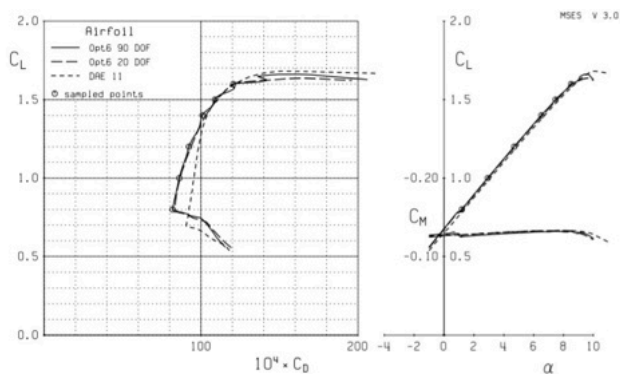


Figure 6: Polars for original DAE-11 airfoil and 6-point optimized airfoils

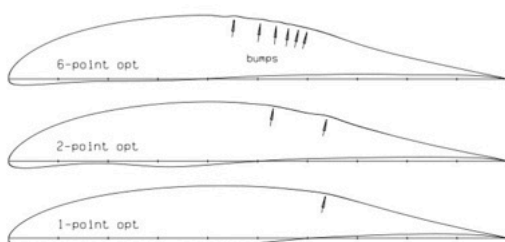


Figure 7: Geometries of optimized airfoils, showing surface bumps.

Adding more point optimisations produces wiggly surfaces.

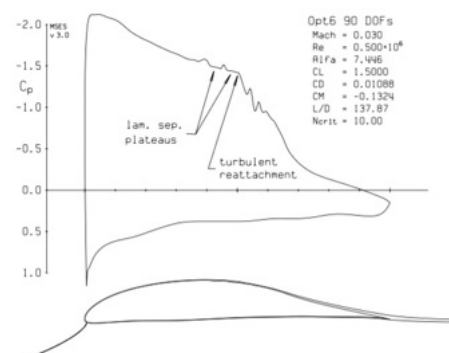


Figure 9: Viscous C_p for 6-point optimized airfoil at sampled point $C_L = 1.5$

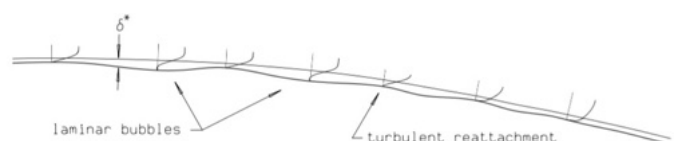
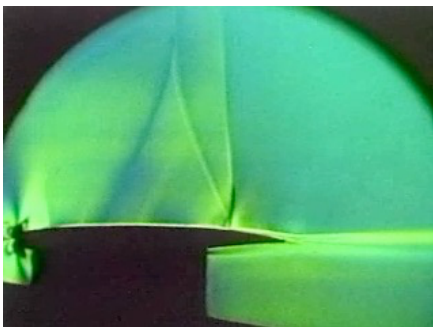


Figure 10: Velocity profiles for 6-point optimized airfoil at $C_L = 1.5$, showing second bump "catching" reattaching shear layer.

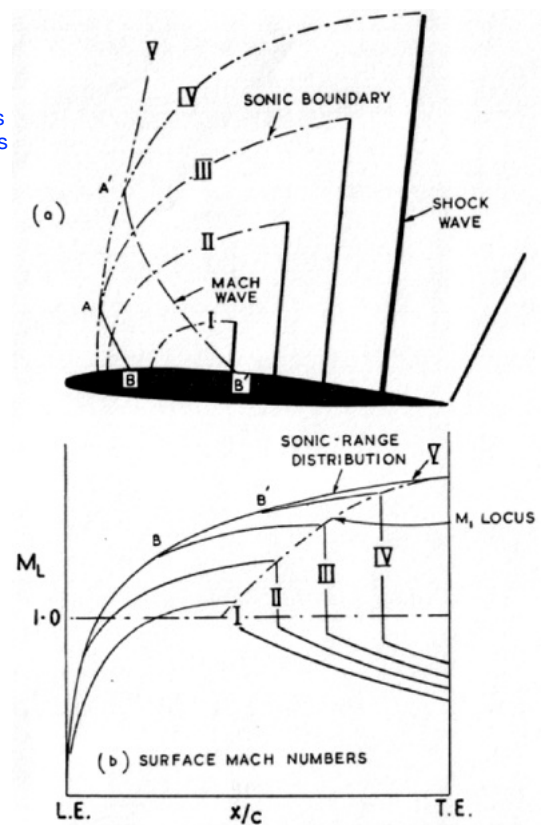
Airfoil design for transonic flight

Design of airfoils for transonic flow — 1



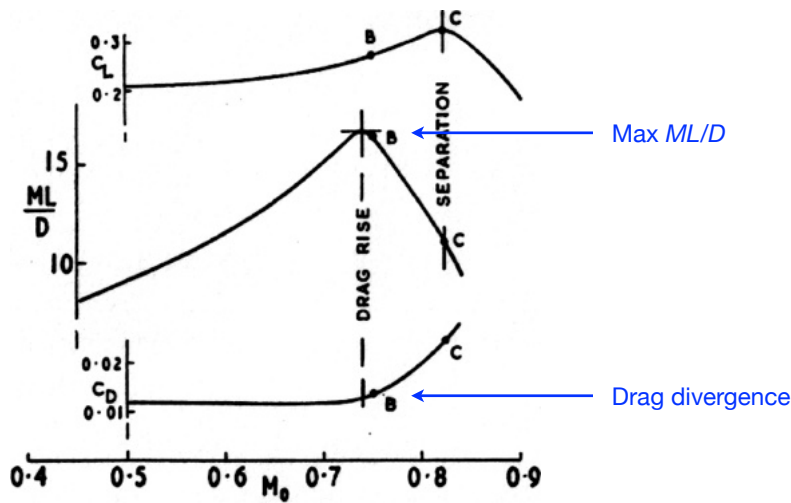
Shock wave is born near point of minimum C_p , moves downstream and strengthens with increasing M_∞ .

When $M_\infty > 1$, a bow shock also appears.



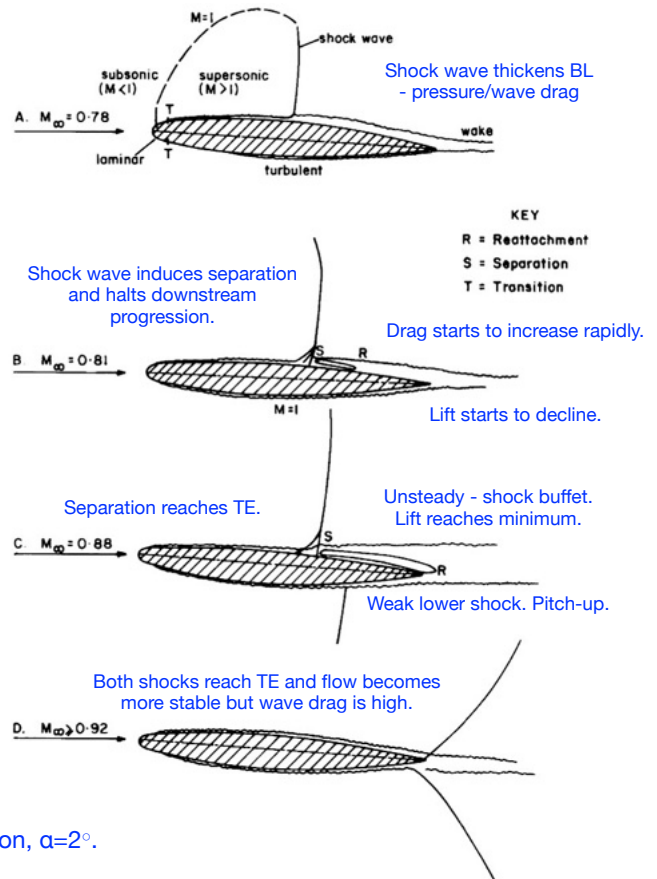
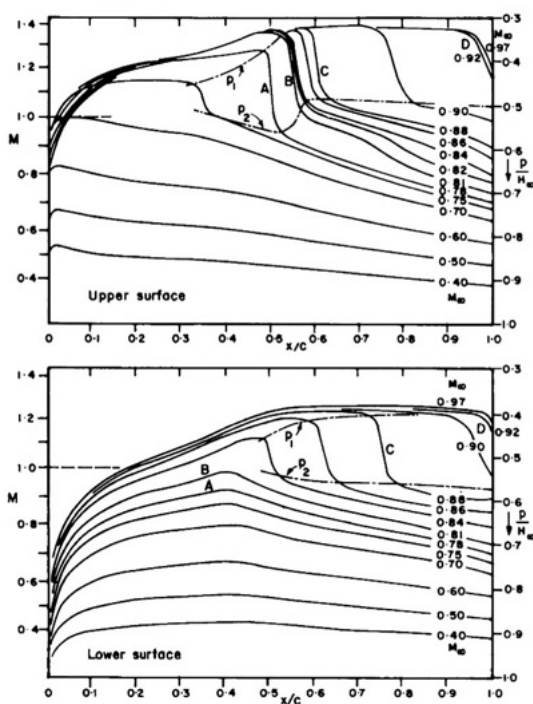
The need

For steady cruise of jet aircraft (fuel consumption rate proportional to thrust),
the range parameter ML/D reaches a maximum at transonic speed.



1. Range requirements may promote the need to postpone transonic drag divergence.
2. Local transonic flow is possible even at low Mach number if C_p is low (e.g. LE slats at landing).
3. Common for helicopter blades, propellers and in turbomachinery.
4. Military aircraft often must negotiate transonic speeds or fly manoeuvres that produce them.

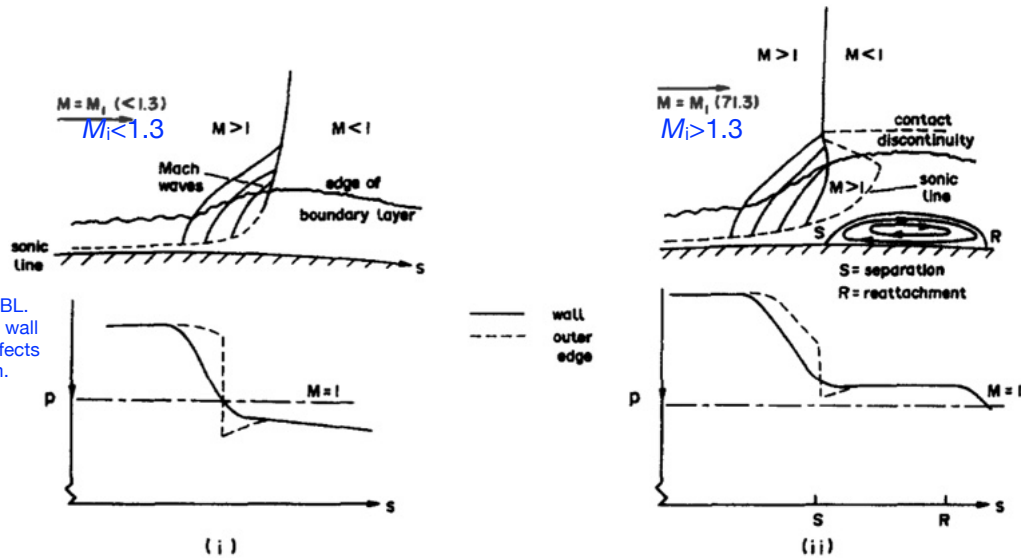
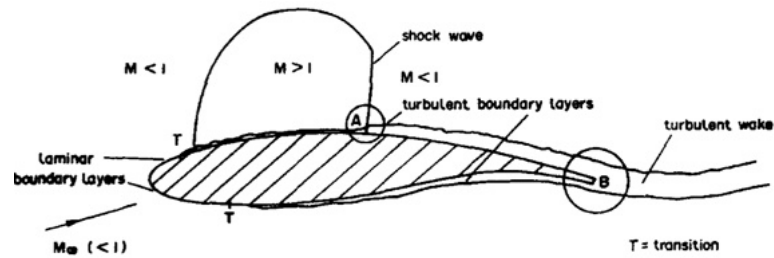
Transonic flow phenomena



10% thick section, $\alpha=2^\circ$.

Shock wave/BL interaction

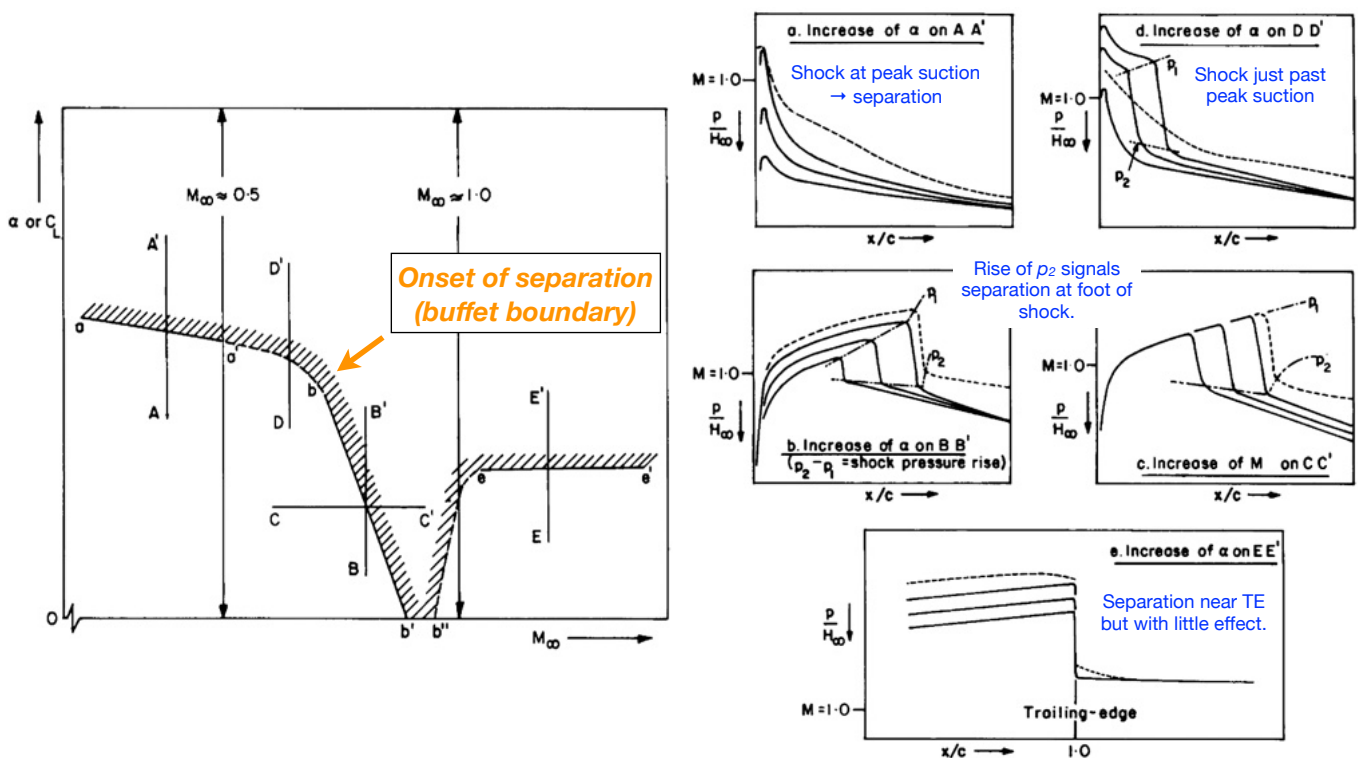
Typically for transonic flows, Reynolds numbers are high enough that BL transition occurs upstream of where any shock wave is encountered.



Flow is sonic within BL. Subsonic region near wall allows shock wave effects to reach upstream.

Rule of thumb: to avoid separation, the local Mach number should not exceed $M=1.3$.

Onset of separation boundary



Dashed lines show distributions when separation is present.

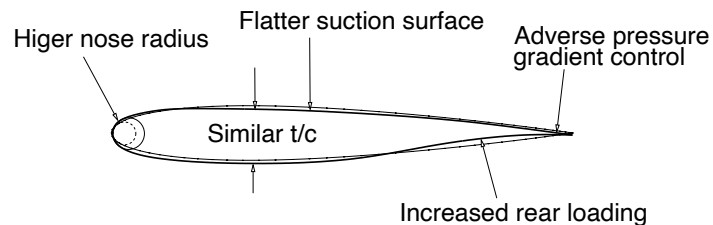
Airfoil design for transonic cruise — 1

Purpose: obtain high lift with small wave drag penalty.

Possible objectives:

1. Thick airfoils to reduce minimum C_p near LE. Also to provide fuel volume and structural strength and stiffness.
2. Aim for shockless flow or flow with weak shock waves.
3. Load the lower surface near nose (reduce y/c) to provide lift and positive pitching moment.
4. Forward shocks tend to produce less drag than aft shocks. “Peaky” airfoils are designed with forward shocks.
5. Ensure that sufficient lift is carried forward on the upper surface as the peak suction near the nose decreases as Mach number increases.
6. If lift is reduced near the nose by flattening the upper surface profile to weaken shock wave, it can be recovered by increasing rear camber. This is the basis of “supercritical” airfoil design.

Comparison of geometry of supercritical airfoils and conventional airfoils

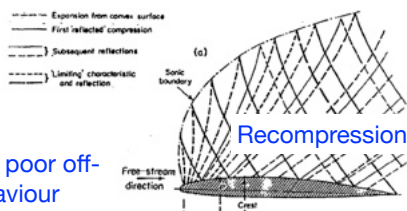


Airfoil design for transonic cruise — 2

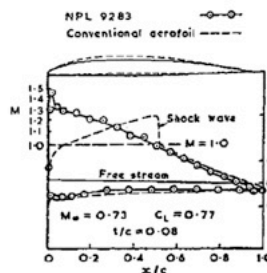
Historical progression

1. ‘**Peaky**’ airfoils: bring upper surface flow to supersonic peak near LE, achieve isentropic recompression to subsonic without shock.

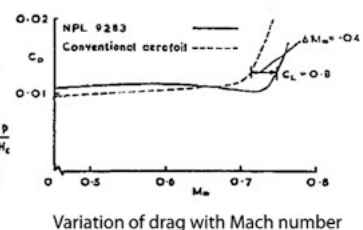
Circa late 1950s



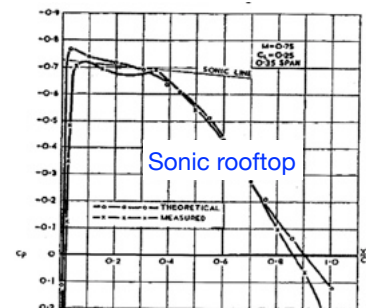
Rather thin, poor off-design behaviour



A shock-free airfoil (peaky)



Variation of drag with Mach number



2. ‘**Sonic rooftop**’ airfoils: bring upper surface flow to sonic near LE and maintain it as far as possible, then recompress with no, or only weak, shock.

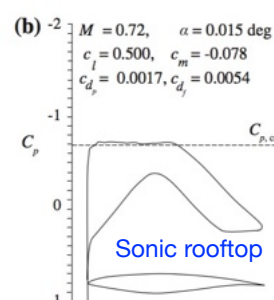
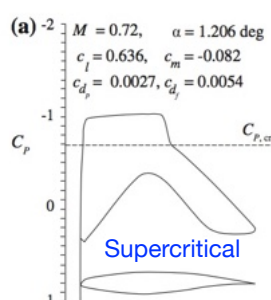
Circa early 1960s

Better. Rear lower surface camber also used to help improve lifting capacity.

3. ‘**Supercritical**’ airfoils: bring upper surface flow to supersonic near LE and maintain that until terminated by relatively weak shock.

Circa 1970 to present

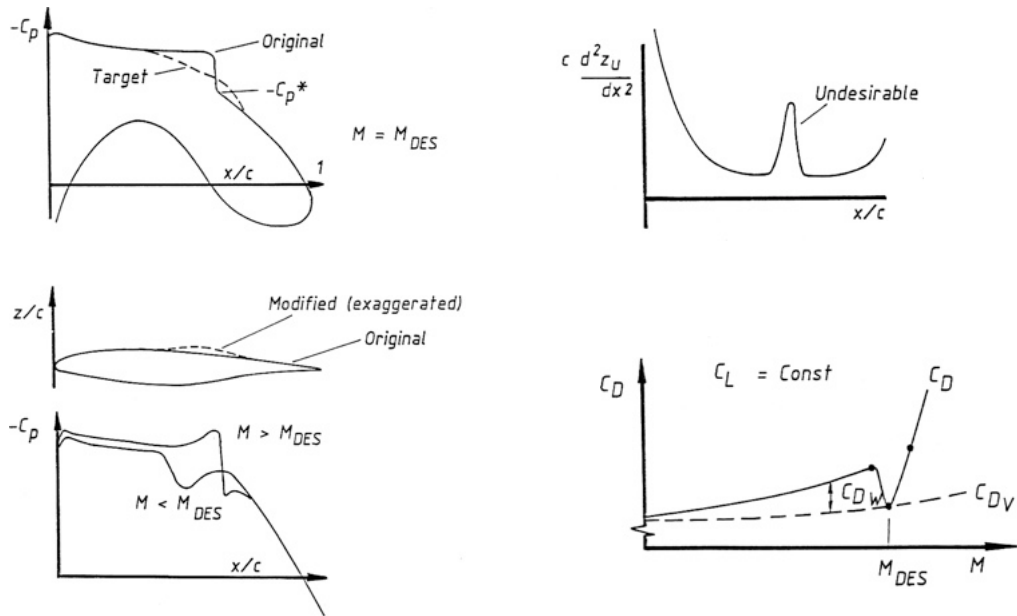
Benefits: more suction/lift than sonic-rooftop, airfoil can be thicker for same lift and drag at equivalent Mach.



Airfoil design for transonic cruise — 3

Potential problems:

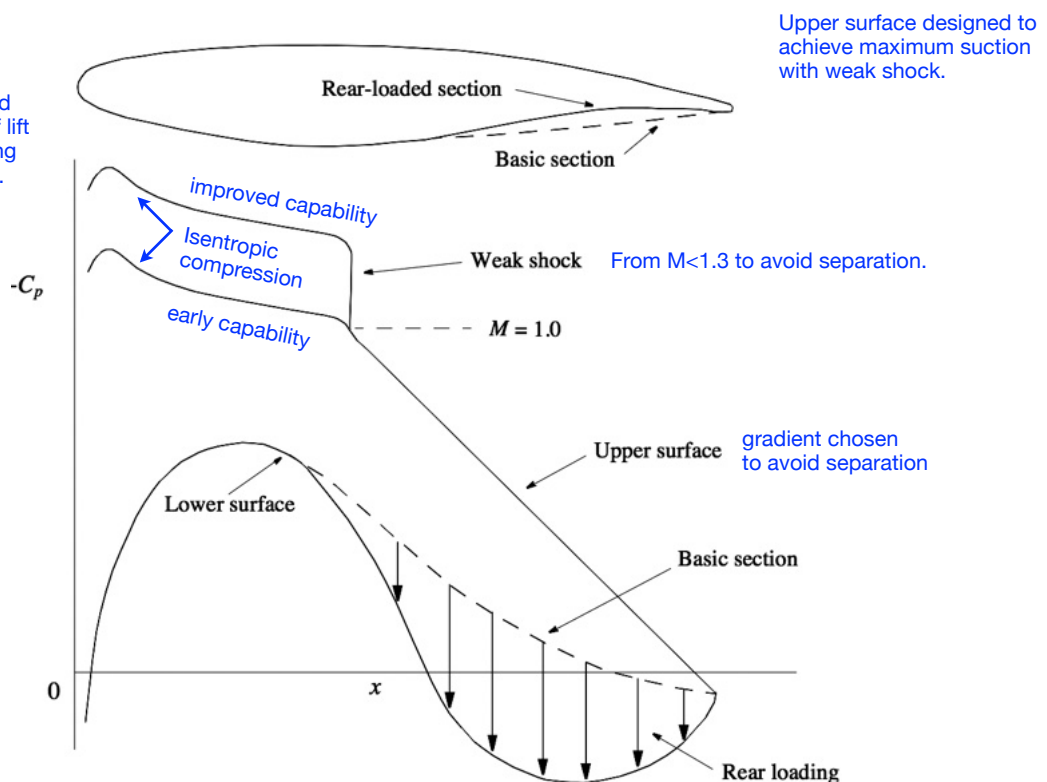
1. The adverse pressure gradient on the aft lower surface can produce separation.
2. Rear loading/camber may cause substantial negative pitching moment, ultimately increasing trim drag and structural weight penalty.
3. Thin trailing edges may be difficult to manufacture.
4. Beware of performance sensitivity to off-design conditions.



Design guidelines — 1

1. Governing equations are nonlinear - analysis requires CFD (e.g. ESDU VGK).
2. Typically the upper and lower surface shapes are considered separately at the design point.

Lower surface typically maximizes thickness and compensates for loss of lift at this point by increasing load carried towards TE.

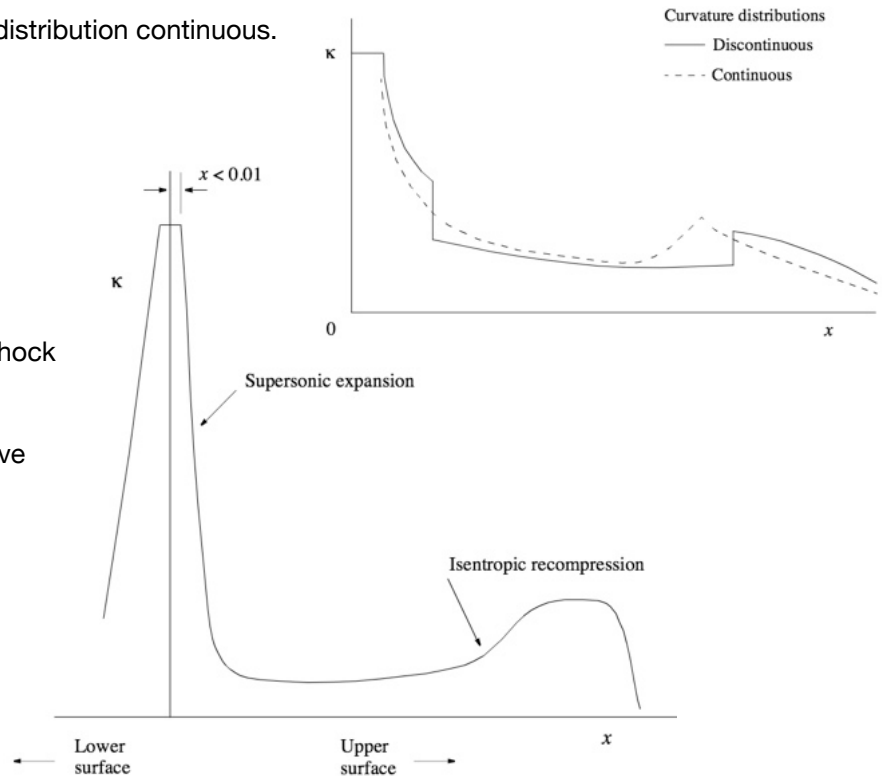


Design guidelines — 2

1. Surface curvatures are used to control flows approximately independently on upper and lower surfaces.
2. Curvature $\kappa = \pm d(\sin\theta)/dx$ where $\sin\theta$ is local airfoil surface slope. $\kappa \approx \pm d^2z/dx^2$ away from LE.
3. Best to keep surface curvature distribution continuous.

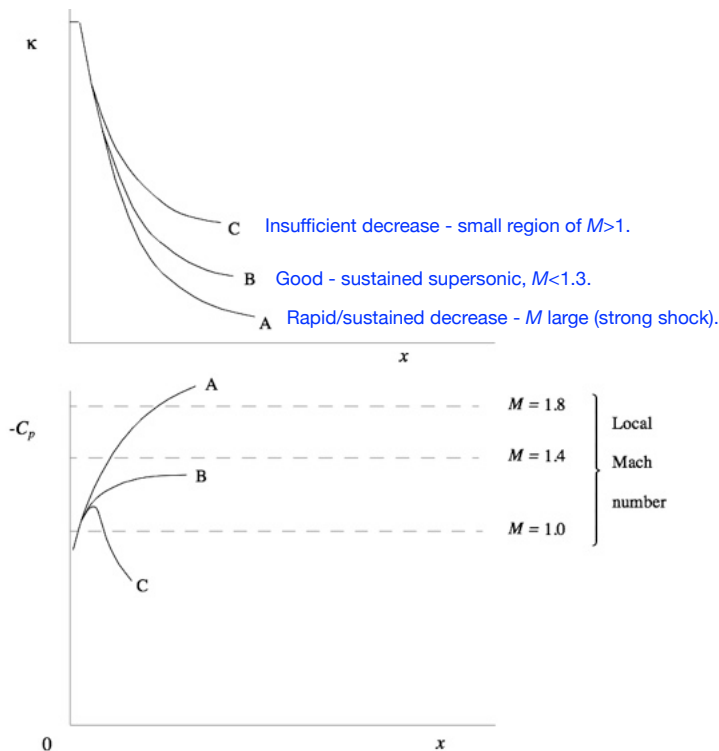
4. Typical curvature distribution attempts to:

- a. accelerate to supersonic around LE;
- b. hold supersonic as far as possible (large suction)
- c. terminate by compressing isentropically or via weak shock to sonic conditions
- d. continue recompression subsonically to small positive C_p at TE

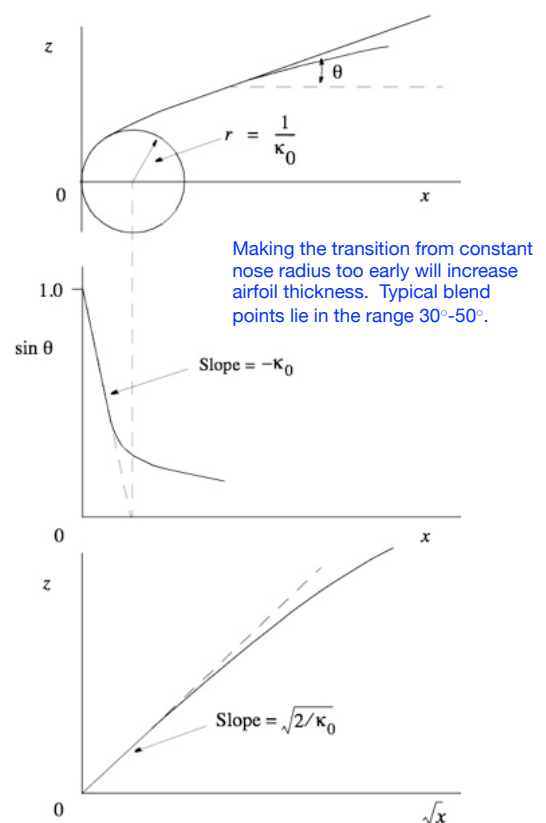


Design guidelines — 3

1. Effect of curvature near LE

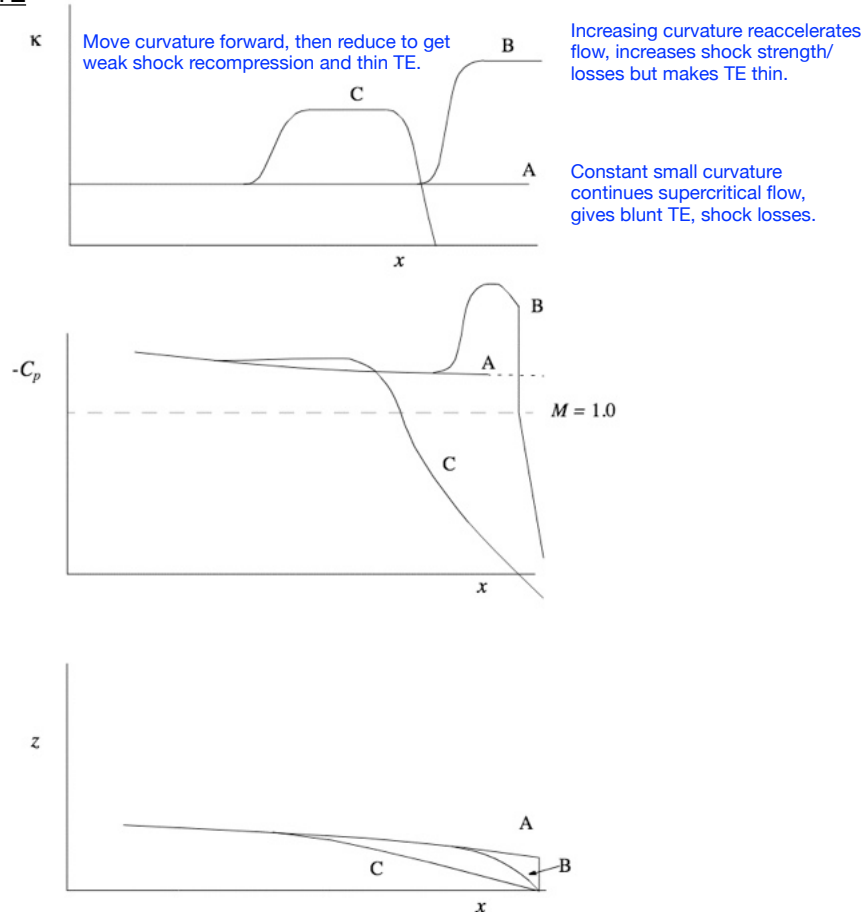


2. Effect of LE radius blend point.



Design guidelines — 4

3. Effect of curvature near TE



Design guidelines — 5

Example camber lines for conventional and supercritical airfoils

